

1 **IFI16 directly senses viral RNA and enhances RIG-I transcription**
2 **and activation to restrict influenza virus infection**

3
4 Zhimin Jiang^{1#}, Fanhua Wei^{2#*}, Yuying Zhang³, Tong Wang¹, Weihua Gao¹, Shufang
5 Yu², Honglei Sun¹, Juan Pu¹, Yipeng Sun¹, Mingyang Wang¹, Qi Tong¹, Chengjiang
6 Gao⁴, Kin-Chow Chang⁵, Jinhua Liu^{1*}

7
8 ¹ Key Laboratory of Animal Epidemiology and Zoonosis, Ministry of Agriculture,
9 College of Veterinary Medicine and State Key Laboratory of Agrobiotechnology,
10 China Agricultural University, Beijing 100094, China;

11 ² College of Agriculture, Ningxia University, Yinchuan 750021, China;

12 ³ School of Biological Science and Technology, University of Jinan, Jinan 250022,
13 China;

14 ⁴ Key Laboratory of Infection and Immunity of Shandong Province & Department of
15 Immunology, School of Biomedical Sciences, Shandong University, Jinan 250012,
16 China;

17 ⁵ School of Veterinary Medicine and Science, University of Nottingham, Sutton
18 Bonington Campus, United Kingdom.

19

20 # These authors contributed equally.

21 * Corresponding author. E-mail: weifanhua999@163.com; ljh@cau.edu.cn.

22

23
24
25
26
27
28
29
30
31
32
33
34
35
36
37
38
39
40
41
42
43
44

Abstract

The Retinoic acid-inducible gene I (RIG-I) receptor senses cytoplasmic viral RNA and activates type I interferons (IFN-I) and downstream antiviral immune responses. How RIG-I binds to viral RNA and how its activation is regulated remains unclear. Here, using IFI16 knockout cells and p204- deficient mice, we demonstrated that the DNA sensor IFI16 enhances IFN-I production to inhibit IAV replication. IFI16 positively upregulates RIG-I transcription through direct binding to and recruitment of RNA Pol II to the RIG-I promoter. IFI16 also binds to influenza viral RNA via its HINa domain, and to RIG-I protein with its PYRIN domain, thus promoting IAV-induced K63- linked polyubiquitination and RIG-I activation. Our work demonstrate that IFI16 is a positive regulator of RIG-I signaling during influenza virus infection, highlighting its role in RLR-mediated innate immune response to IAV and other RNA viruses, and suggesting its possible exploitation to modulate the antiviral response.

Keywords: Influenza virus; RNA recognition; IFI16; RIG-I; type I interferons

45 **Introduction**

46 Influenza virus is one of the most important causes of respiratory tract infection,
47 resulting in at least 26 million influenza illnesses, 250,000 hospitalizations and 14,000
48 deaths during the 2019-2020 season in the United States
49 (<https://www.cdc.gov/flu/season/index.html>). A(H1N1)/pdm2009, H3N2, and
50 influenza B (B/Yamagata or B/Victoria lineage) viruses are mainly responsible for
51 seasonal influenza epidemics each year. Moreover, avian influenza virus remains a
52 significant additional threat to human health, in particular the H5, H7 and H9
53 subtypes. Although vaccination is the most effective way to control IAV, prediction of
54 evolving immunogenic epitopes as well as challenges of vaccine production and
55 distribution often limit vaccine efficacy and availability. Furthermore, antiviral
56 resistant IAV strains continued to be identified; they include H274Y mutation in the
57 neuraminidase (NA)^{1,2}, and three major mutations (L26F, V27A, and S31N) in the M2
58 protein^{3,4}. Hence, the development of effective interventions against influenza virus
59 infection remains an outstanding public health need. Targeting an essential host factor
60 critical for influenza infection is a promising antiviral strategy⁵.

61 Several families of pattern recognition receptors (PRRs) have been described:
62 toll like receptors (TLRs), retinoic acid inducible gene-I (RIG-I) receptors (RLRs) and
63 nucleotide oligomerization domain (NOD)-like receptors (NLRs) are involved in the
64 recognition of influenza viruses⁶⁻⁸. Among them, RIG-I is thought to be the most
65 important sensor of influenza virus⁹; it binds the 5'ppp-RNA of the virus, leading it to
66 undergo conformational changes and exposing its caspase activation and recruitment

67 domains (CARDs)¹⁰, which is then ubiquitinated by the action of E3 ligases such as
68 tripartite motif 25 (TRIM25)¹¹ and RIPLET¹². TRIM25 activates RIG-I through the
69 generation of unanchored K63-linked polyubiquitin chains interacting with the
70 CARDs¹³, or through the generation of anchored K63-linked polyubiquitin chains
71 attached to lysine 172 of RIG-I¹¹. This process results in the interaction of RIG-I with
72 the mitochondrial antiviral signaling (MAVS) adaptor, which leads to the subsequent
73 activation of IRF3/7 and NF- κ B and thereby inducing the expression of IFN-I and
74 pro-inflammatory cytokines¹⁴. Therefore, RIG-I activation has to be tightly regulated
75 to ensure effective virus inhibition with minimal excessive inflammatory response.

76 Interferon- γ -inducible protein-16 (IFI16) is a member of the pyrin and HIN
77 domain (PYHIN) containing protein family, which encodes a class of homologous
78 proteins that share a 200-amino acid signature motif (HIN)¹⁵. IFI16 was first reported
79 as a sensor of transfected and viral DNA involved in innate signaling^{16,17} and
80 functions as an innate immune sensors in eukaryotic cells¹⁸⁻²⁴. IFI16 senses the
81 double-stranded DNA (dsDNA) from invading DNA viruses including herpes simplex
82 virus 1 (HSV-1), Kaposi sarcoma-associated herpesvirus (KSHV), vaccinia virus
83 (VACV)^{21,24,25}, the single-stranded DNA (ssDNA) from HIV-infected CD⁴⁺ T cells
84 and nuclear damaged DNA from etoposide-treated keratinocytes^{22,26}. DNA
85 recognition by IFI16 induces the activation of the stimulator of interferon
86 genes-TANK-binding kinase 1-interferon regulatory factor 3 (STING-TBK1-IRF3)
87 pathway, leading to the induction of IFN-I or ASC-caspase 1-dependent
88 inflammasome to produce interleukin-1 β (IL-1 β)^{21,24,26}. Additionally, a role for IFI16

89 in RNA virus infection has been identified; IFI16 transcriptionally regulates the IFN-I
90 gene expression in Sendai virus infection²⁷. The murine ortholog of IFI16 (p204) is
91 highly induced in mouse hepatitis coronavirus infection and inhibits IRF7-mediated
92 IFN-I production²⁸. Moreover, it was shown that IFI16 interacts with MAVS to
93 promote MAVS-mediated production of IFN-I that inhibits porcine reproductive and
94 respiratory syndrome virus 2 replication²⁹. More recently, IFI16 was found to directly
95 bind Chikungunya virus (CHIKV) genome RNA and restrict viral replication and
96 maturation³⁰, which further suggests that IFI16 may play a crucial role in RNA virus
97 infection. However, the precise role of IFI16 in influenza virus infection has not been
98 elucidated.

99 Here, we showed that IFI16, which was identified as an influenza viral RBP, was
100 highly induced both *in vitro* and *in vivo* during IAV infection. We further
101 demonstrated that IFI16 upregulated *RIG-I* transcription by binding its HINa domain
102 to the *RIG-I* promoter, and interacted with both IAV vRNAs and RIG-I to promote
103 influenza virus-induced K63-linked polyubiquitination of RIG-I. Collectively, these
104 results indicate that IFI16 is a key positive regulator of RIG-I signaling in antiviral
105 innate immune responses to influenza virus infection.

106

107

108

109

110

111 **Results**

112 **IFI16 is a viral RBP involved in influenza virus infection**

113 Owing to its RNA genome, influenza virus utilizes RNA-binding proteins (RBPs)
114 of both viral and host origin for its replication. To uncover comprehensive viral RNA
115 (vRNA)-host protein interactions, we performed affinity purification coupled with
116 mass spectrometry (AP-MS) analysis of influenza vRNA complexes. The eight vRNA
117 segments of H7N9 virus were individually transcribed and labeled with biotin *in vitro*,
118 and incubated with lysates from IAV virus-infected THP-1 cells. vRNA complexes
119 bound to streptavidin magnetic beads were analyzed by mass spectrometry (Fig.1A).
120 Domain enrichment analysis of co-purified proteins for each RNA bait revealed that
121 more than 90% of the isolated proteins harbored nucleic acid binding domains
122 (Fig.1B). We identified 70 candidate vRNA-binding proteins that could bind to no
123 less than 3 baits. A high number of co-purified proteins have been reported as RBPs,
124 such as PTBP1³¹, TRA2B³², DDX5³³, DDX3X³⁴, and RBBP6³⁵, which indicates that
125 our approach was effective in identifying vRNA-interacting proteins for influenza
126 virus. Expression results demonstrated that *IFI16* was most highly expressed for the
127 duration of IAV infection (Fig.1C) which suggests that IFI16 may play an important
128 role in IAV infection.

129 To determine whether IFI16 is involved in IAV replication, we first evaluated
130 *IFI16* expression in PR8-infected human cells. *IFI16* mRNA level was significantly
131 upregulated in THP-1, A549 and HEK293 cells during PR8 infection (Extended Data
132 Fig.1A-C). We also found that PR8 infection significantly elevated *p204* expression in

133 mice lung tissues at 1 day post infection (dpi), 3 dpi and 5 dpi (Extended Data Fig.1D).
134 PR8 virus actively induced the expression of *IFI16* in THP-1 (Extended Data Fig.1E)
135 and A549 cells (Fig.1D) cells. Furthermore, UV-inactivated PR8 virus did not induce
136 *IFI16* expression in A549 cells compared with live virus infection (Extended Data
137 Fig.1F-G). Collectively, the findings suggest that *IFI16* is involved in the modulation
138 of influenza virus infection.

139 In uninfected cells, IFI16 was mainly localized in the nucleus; PR8 infection
140 induced accumulation of IFI16 in the nucleus and cytoplasm (Fig.1E-F). Consistent
141 with the immunostaining results, PR8 virus infection caused build-up of IFI16 protein
142 in the cytoplasm and nucleus (Extended Data Fig.1H). And treatment of A549 cells
143 with human IFN- γ or Poly(I:C) also induced IFI16 accumulation in the nucleus and
144 cytoplasm (Extended Data Fig.1I-K). It was reported that acetylation of IFI16
145 modulates its cellular distribution and cytoplasm translocation in DNA virus
146 infection^{25,36}. During IAV infection, we also detected the acetylation of IFI16 in PR8
147 virus-infected A549 cells at 12 and 24 hpi (Fig.1G, Extended Data Fig.1L).
148 Additionally, low levels of nuclear acetylated IFI16 PLA dots were detected in
149 uninfected A549 cells (Fig.1H). In contrast, acetylated IFI16 dots were clearly
150 elevated in the nucleus and cytoplasm at 24 hpi (Fig.1H). We found that IAV-induced
151 accumulation of IFI16 into the cytoplasm was abolished in C646-treated cells
152 (Extended Data Fig.1M). Collectively, *IFI16* is highly upregulated during IAV
153 infection and whose associated acetylation could confer functional modification such
154 as stabilization of IFI16 protein.

155 **IFI16 inhibits IAV infection *in vitro* and *in vivo***

156 To determine the impact of IFI16 on influenza virus, *IFI16*-Flag vectors were
157 transfected into A549 cells followed by PR8 infection at 1.0 MOI. Overexpression of
158 IFI16 significantly reduced viral titers of PR8 at 18 hpi (Fig.2A) and reduced the
159 expression of viral NP and M1 proteins (Fig.2B). Increasing the amounts of
160 transfected *IFI16*-Flag vectors in HEK293T-Gluc cells resulted in impaired viral
161 replication in a dose-dependent manner (Fig.2C). In addition, overexpression of IFI16
162 inhibited the expression of mRNA and vRNA of NP and M1 genes in A549 cells
163 (Extended Data Fig.2A), and protein levels of NP at 6, 12 and 18 hpi in HEK293 cells
164 (Extended Data Fig.2B). Conversely, when *IFI16* was knockdown by siRNA in A549
165 cells, there were significant increases in viral protein and titer of progeny viruses
166 (Extended Data Fig.2C-D). To investigate the function of endogenous IFI16 during
167 IAV infection, *IFI16*^{+/+} and *IFI16*^{-/-} A549 cells were infected with PR8 virus. Infected
168 *IFI16*^{-/-} A549 cells produced higher viral titers at 12 and 24 hpi (Fig.2D) and protein
169 levels of viral NP and M1 at 12 and 18 hpi (Fig.2E). In a gain-of-function experiment,
170 exogenous expression of IFI16 in *IFI16*^{-/-} A549 cells effectively reduced the
171 expression of viral NP and M1 proteins at 12 and 18 hpi (Fig.2F). Accordingly, we
172 found that the replication of GFP-tagged PR8 virus was markedly increased in *IFI16*^{-/-}
173 A549 cells compared with *IFI16*^{+/+} A549 cells (Fig.2G). Collectively, these findings
174 indicate that IFI16 inhibits influenza virus replication in human cells.

175 Additionally, PR8-infected WT mice suffered significantly less weight loss than
176 *p204*-deficient (KO) mice, and started to regain body weight by 8 dpi (Fig.3A).

177 Consequently, survival rate of PR8 infected *p204*^{-/-} mice was significantly poorer than
178 infected WT mice (Fig.3B), which suggests that control of IAV infection *in vivo* also
179 requires *p204*. In lung tissues of KO mice, PR8 virus replication at 4 and 6 dpi was
180 higher (Fig.3C), with accompanying greater viral NP mRNA and vRNA levels
181 (Fig.3D), in lung tissues of KO mice than in corresponding WT mice. Moreover, viral
182 NP staining was more intense in lung sections of KO mice at 5 dpi than in
183 corresponding WT mice (Fig.3E). Notably, gross- and histo-pathology revealed that
184 lung tissues of PR8 virus-infected KO mice displayed more extensive damage at 3
185 and 5 dpi (Fig.3F), and more severe inflammatory damage at 3 dpi (Fig.3G), than in
186 corresponding WT mice. Accordingly, IL-6 and MCP-1 proteins in BALFs were also
187 significantly higher in PR8-infected WT mice than those found in corresponding
188 *p204*^{-/-} mice (Fig.3H-I). Furthermore, *p204* deficiency dramatically inhibited their
189 transcription: *IFN-β*, *viperin*, *OAS1*, *ISG15* and *IL-6* in PR8 virus-infected BMDMs
190 (Fig.3J-N). Therefore, IFI16 is required for host defense against influenza virus
191 infection *in vitro* and *in vivo*.

192 **IFI16 enhances the production of IFN-I in IAV infection**

193 DNA recognition by IFI16 induces the activation of STING-TBK1-IRF3
194 pathway, leading to the induction of IFN-I^{21,24,26}. To investigate innate immune
195 activation by IFI16, we performed transcriptomic analysis in *IFI16*^{+/+} and *IFI16*^{-/-}
196 A549 cells infected with PR8 virus for 12 h. In GO-term enrichment analysis, 10
197 enriched terms identified were related to antiviral responses (Fig.4A). The number of
198 genes associated with individual terms as well as enrichment probability were lower

199 in *IFI16*^{-/-} A549 cells (Fig.4A). Sixteen ISGs were found to be exclusively
200 upregulated in *IFI16*^{+/+} cells during IAV infection, while only 4 ISGs were
201 upregulated in *IFI16*^{-/-} A549 cells (Fig.4B). Collectively, these results show that the
202 induction of ISGs was reduced in the absence of IFI16. We next evaluated the
203 function of IFI16 in the induction of IFN-I. RT-qPCR analysis showed that
204 overexpression of *IFI16* enhanced PR8 virus-induced expression of *IFN-β*, *ISG15* and
205 *IL-6* at 6 and 12 hpi (Extended Data Fig.3A-C). Conversely, IFI16 deficiency greatly
206 reduced the PR8 virus-induced expression of *IFN-β*, *RIG-I*, *ISG56*, and *viperin*
207 (Fig.4C-F) as well as *IFN-α4*, *IRF7* and *CXCL5* (Extended Data Fig.3D-F) in A549
208 cells. Furthermore, overexpression of IFI16 in A549 cells increased PR8
209 virus-induced IFN-β protein production at 12 and 18 hpi in a dose-dependent manner
210 (Fig.4G), while IFI16 deficiency markedly decreased IFN-β production (Fig.4H),
211 which suggest that IFI16 mediates antiviral effects through influenza virus-induced
212 IFN-I signaling.

213 To examine the contribution of IFI16 to the RIG-I signaling, we transfected
214 *IFI16*-Flag or control plasmids into A549 cells followed by infection with PR8 virus
215 at 1.0 MOI. Overexpression of IFI16 in infected cells enhanced protein detection of
216 RIG-I, phosphorylated (p)-TBK1, p-IRF3 and p-P65 relative to infected controls
217 (Fig.4I). In contrast, deficiency of IFI16 in infected cells led to reduced protein
218 detection of RIG-I, p-TBK1 and p-IRF3 compared with the *IFI16*^{+/+} group (Fig.4J).
219 Consistent with these results, overexpression of IFI16 in the presence of 5'ppp-RNA
220 also increased protein detection of RIG-I, p-TBK1 and p-IRF3 (Extended Data

221 Fig.3G). Furthermore, exogenous expression of IFI16 in infected *IFI16*^{-/-} A549 cells
222 restored the protein expression of RIG-I, p-TBK1 and p-IRF3 (Extended Data Fig.3H).
223 Immunofluorescence results showed that IFI16 deficiency reduced the level of p-IRF3
224 (Ser396) in nuclear in PR8 virus-infected A549 cells (Fig.4K-L). Taken together,
225 these findings indicate that IFI16 is a potent stimulator of the IFN-I response in
226 influenza virus infection.

227 **IFI16 transcriptionally upregulates the expression of *RIG-I***

228 Overexpression of IFI16 progressively upregulated RIG-I protein expression in
229 A549 cells in a time-dependent manner (Fig.5A) and in a dose-dependent manner
230 (Extended Data Fig.4A). HEK293 cells co-transfected with *IFI16*-Myc and
231 *RIG-I*-Flag followed by cycloheximide (CHX) treatment did not exhibit evidence of
232 RIG-I protein degradation (Extended Data Fig.4B). And overexpression of IFI16 also
233 increased protein and mRNA expression of RIG-I in *ifnar1*^{-/-}A549 cells in a
234 dose-dependent manner (Extended Data Fig.4C-4D). Furthermore, A549 cells
235 transfected with *IFI16*-Flag vectors showed rising levels of *RIG-I* mRNA in a
236 vector-dose dependent manner (Extended Data Fig.4E) and a progressive
237 time-dependent manner (Fig.5B). Consistent with the findings in A549 cells, mRNA
238 expression of *RIG-I* in PR8 virus infected lung tissues of *p204*-deficient (KO) mice
239 was significantly reduced at 1 and 3 dpi compared with corresponding WT mice
240 (Extended Data Fig.4F). Taken together, our results indicate that IFI16 upregulates
241 *RIG-I* from the transcriptional level.

242 To further assess the role of IFI16 in the regulation *RIG-I*, luciferase reporter

243 vector driven by a *RIG-I* promoter was used in transfections of HEK293 cells. The
244 *RIG-I* promoter was responsive to IFI16 overexpression in a vector-dose dependent
245 manner (Fig.5C), which indicates that IFI16 is capable of transactivating the *RIG-I*
246 promoter.

247 To determine the minimum promoter length of *RIG-I* that is responsive to the
248 IFI16 induction, an extensive series of *RIG-I* promoter deletion constructs, each
249 spliced to luciferase reporter gene, were generated for co-transfections with increasing
250 amounts of *IFI16*-Flag expression vectors (Fig.5D-I). The minimum *RIG-I* promoter
251 responsive to *IFI16*-Flag overexpression was found to be between -371 to -360 bp in
252 length (Fig.5I). Furthermore, Flag antibody pull down experiments, based on a series
253 biotinylated double-stranded DNA probes that spanned the minimum promoter
254 section (Extended Data Fig.4G), found that only probe p2-mut4 which harbored
255 mutations between the -371 to -360 region of the promoter failed to bind IFI16-Flag
256 (Extended Data Fig.4H). CHIP-qPCR assays, using two sets of primer pairs that target
257 the -500 to -250 bp region of *RIG-I* promoter, further demonstrated direct binding of
258 IFI16 to the *RIG-I* promoter (Fig.5J). Collectively, IFI16 is capable of binding to the
259 *RIG-I* promoter to promote *RIG-I* transcription.

260 Next, to determine whether IFI16 affects the recruitment of RNA Pol II to the
261 *RIG-I* promoter, chromatin immunoprecipitation was performed with Pol II antibody
262 on *IFI16*^{+/+} and *IFI16*^{-/-} A549 cells, infected with PR8 virus at 1.0 MOI for 0 and 12 h.
263 qPCR targeting the detection of the basal promoter site of *RIG-I* showed more RNA
264 Pol II binding to the basal promoter of infected *IFI16*^{+/+} than infected *IFI16*^{-/-} A549

265 cells (Fig.5K), but no significant difference on the GAPDH promoter (Extended Data
266 Fig.4I), suggesting that during infection IFI16 facilitates RNA Pol II recruitment to
267 the basal promoter of *RIG-I*.

268 To investigate the domain(s) in IFI16 responsible for activating *RIG-I*
269 transcription, we constructed *IFI16* expression mutants bearing different domain
270 deletions (Extended Data Fig.4J). Mutants without the HINa domain completely lost
271 the ability to activate the *RIG-I-luc* reporter gene (Fig.5L). In a separate experiment,
272 we also found that in the absence of the HINa domain there was no binding of IFI16
273 to biotinylated *RIG-I* promoter (Extended Data Fig.4K). Deletion of HINa domain in
274 IFI16 abrogated its antiviral activity in response to PR8 virus infection (Extended
275 Data Fig.4L). Taken together, IFI16 binds *RIG-I* promoter with its HINa domain
276 facilitating the recruitment of RNA Pol II to the site, thereby enhancing the
277 transcriptional activation of *RIG-I*.

278 **IFI16 binds vRNAs and interacts with RIG-I**

279 Since IFI16 is also a RBP, we determined if IFI16 binds vRNAs as with *RIG-I*
280 promoter. Pull down assays using cell lysates of HEK293 cells, separately
281 overexpressing Flag-tagged IFI16, RIG-I, MDA-5 and TBK1 proteins, incubated with
282 biotinylated NP vRNA showed binding of IFI16, RIG-I and MDA-5 to the vRNAs
283 (Extended Data Fig.5A). MST results showed that the HINa domain also exhibited
284 high affinity for full-length NS vRNA (Extended Data Fig.5B). To further
285 demonstrate binding between IFI16 and other IAV RNAs, purified GST-IFI16
286 proteins were incubated with fluorescein-labeled HA, NP, PA and PB2 vRNAs. MST

287 assays also showed IFI16 binding with the different vRNAs (Extended Data Fig.5C).
288 Furthermore, RNA FISH analysis revealed increasing co-localization of IFI16 with
289 NP vRNA in PR8 virus-infected A549 cells at 6 and 12 hpi (Fig.6A). To identify
290 bound vRNAs during infection, RNA eluted from co-precipitation of *IFI16*-Flag from
291 IAV-infected *RIG-I*^{-/-} cells was subjected to deep sequencing analysis which detected
292 IFI16 binding to all eight IAV gene segments (Fig.6B). RIG-I has been found with
293 IAV genomic fragments³⁷. IFI16 was also specifically enriched in genomic IAV
294 segments during infection (Fig.6B). Importantly, only wild-type IFI16 and IFI16
295 mutants bearing the HINa domain associated with vRNA fragments during infection
296 (Fig.6C, Extended Data Fig.5D-E). Taken together, these results indicate that during
297 infection IFI16 can directly bind viral genome RNAs via its HINa domain.

298 To determine if IFI16 is involved in the recognition of vRNAs by RIG-I during
299 influenza virus infection, co-IP assays were performed that demonstrated the
300 endogenous interaction of IFI16 and RIG-I during PR8 virus infection in A549 cells
301 (Fig.6D-E). Furthermore, *in situ* PLA microscopy showed co-localization of IFI16
302 and RIG-I in the cytoplasm of PR8 virus-infected A549 cells (Fig.6F). Consistent with
303 PLA results, confocal microscopy also found increasing interaction between IFI16
304 and RIG-I during IAV infection (Extended Data Fig.5F). The PYRIN domain can
305 mediate the interaction between IFI16 and host proteins^{38,39}. The IFI16- Δ PYRIN-GFP
306 mutant was unable to co-localize with RIG-I in HEK293 cells, indicating that the
307 PYRIN domain is required in the protein-protein interaction (Extended Data Fig.5G).
308 Interestingly, *PYRIN*-GFP transfection into HEK293 cells resulted in its protein

309 co-localization with RIG-I that formed filamentous structures (Extended Data Fig.5H
310 -I). IFI16 filamentous structures are involved in antiviral responses by associating
311 with host restriction factors⁴⁰⁻⁴². Collectively, these findings indicate that IFI16 binds
312 influenza viral RNAs and associates with RIG-I in influenza virus-infected cells.

313 **RIG-I is required for IFI16-mediated antiviral response in IAV infection**

314 K63-linked polyubiquitination of RIG-I by TRIM25 is essential for its
315 activation¹¹. To explore the potential role of IFI16 in the promotion of RIG-I signaling,
316 we examined the interaction between TRIM25 and RIG-I in PR8 virus-infected
317 *IFI16*^{+/+} and *IFI16*^{-/-} A549 cells. Co-IP and *in situ*-PLA experiments indicated that
318 IFI16 deficiency impaired the interaction and co-localization between RIG-I and
319 TRIM25 due to their reduced expression in infected *IFI16*^{-/-} cells, and inhibited
320 K63-linked polyubiquitination of RIG-I during virus infection (Extended Data
321 Fig.6A-B, 7A). To further determine the impact of IFI16 on RIG-I polyubiquitination,
322 we transfected HEK293 cells with Myc control or *IFI16*-Myc, *RIG-I*-Flag,
323 *TRIM25*-His and either HA-ubiquitin, HA-ubiquitin-K48 or HA-ubiquitin-K63
324 plasmids. Co-IP experiments showed that IFI16 remarkably enhanced the interaction
325 between TRIM25 and RIG-I and promoted RIG-I polyubiquitination in the presence
326 of HA-ubiquitin and HA-ubiquitin-K63, but not HA-ubiquitin-K48 (Extended Data
327 Fig.7B). Thus, IFI16 facilitates TRIM25 binding to RIG-I and consequently
328 promotes K63-linked polyubiquitination of RIG-I. RIP-RT-qPCR assays showed that
329 overexpression of IFI16 significantly enhanced the RIG-I binding to PA vRNA
330 (Extended Data Fig.7C). And correspondingly, IFI16 deficiency also markedly

331 reduced RIG-I binding to PA vRNA in PR8 virus-infected A549 cells (Extended Data
332 Fig.7D). RIP-EMSA and RNA pull-down experiments further demonstrated that the
333 binding of PA vRNA with RIG-I is sharply increased with increasing amount of IFI16
334 (Extended Data Fig.6C-6D). Furthermore, RNA co-purified with RIG-I by RIP
335 analysis from IAV-infected *IFI16*^{+/+} cells could induce the production of IFN- β more
336 effectively than that from *IFI16*^{-/-} cells (Extended Data Fig.7E-F), suggesting that
337 IFI16 facilitates the stable binding of RIG-I to vRNAs during IAV infection.
338 Importantly, only wild-type IFI16 and IFI16 mutants bearing HINa and PYRIN
339 domain, but not HINb, promoted vRNA binding to RIG-I (Extended Data Fig.6E) and
340 enhanced the production of IFN- β during IAV infection (Extended Data Fig.6F).
341 Consistent with these observations, IFN- β reporter assays showed that overexpression
342 of IFI16 significantly enhanced PR8 virus-induced expression of IFN- β -luciferase
343 reporter genes (Extended Data Fig.7G). Moreover, RIG-I-induced activity of
344 IFN- β -luciferase reporter rose with increasing amounts of IFI16 expression vectors
345 used in transfections (Extended Data Fig.7H). Taken together, these results suggest
346 that IFI16 promotes the activation of RIG-I signaling and in so doing, boosts the
347 production of IFN-I.

348 Finally, to investigate whether antiviral function of IFI16 in IAV infection is
349 dependent on RIG-I, A549 cells were transfected with the *RIG-I*- or *MAVS*-targeting
350 siRNAs and then infected with IAV. Western blotting showed that the level of RIG-I
351 or MAVS was significantly reduced by *RIG-I*-targeting siRNA#2835 (Extended Data
352 Fig.7I) or *MAVS*-targeting siRNA#571 transfection (Extended Data Fig.6G). IAV

353 infection could not effectively stimulate the production of IFN- β in *RIG-I*- or
354 *MAVS*-silenced *IFI16*^{+/+} A549 cells (Extended Data Fig.6H, 7J). Overexpression of
355 IFI16 in *RIG-I*- or *MAVS*-silenced A549 cells could not induce the production of
356 IFN- β during IAV infection (Extended Data Fig.6I, 7K). Additionally, *RIG-I*^{-/-}
357 HEK293 cells were transfected with *IFI16*-Flag or Flag vectors and then infected with
358 PR8 virus at 1.0 MOI. Overexpression of IFI16 failed to inhibit viral NP and M1
359 replication in PR8 virus-infected *RIG-I*^{-/-} cells at 6 and 12 hpi (Extended Data Fig.7L),
360 whereas exogenous expression of RIG-I in *RIG-I*^{-/-} cells rescued the inhibitory effect
361 of IFI16 on viral titers at 24 hpi (Extended Data Fig.7M). Taken together, our results
362 indicate that the antiviral function of IFI16 is dependent on RIG-I.

363

364

365

366

367

368

369

370

371

372

373

374

375 **Discussion**

376 Host cells possess critical sensors that can discriminate viral and host nucleic
377 acids. IFI16 has been demonstrated to be a sensor of viral DNA in innate immune
378 signaling^{16,17}. However, its role in sensing viral RNA during infection, in particular
379 influenza virus infection, hitherto is unknown. In this study, we demonstrated that
380 IFI16 is a viral RBP and is induced during influenza virus infection. IFI16 inhibited
381 influenza virus replication in human cell lines and in mice through enhanced the
382 induction of IFN-I. IFI16 enhances the transcription of *RIG-I*, binds viral RNAs and
383 interact with RIG-I protein, thereby increasing the sensitivity of RIG-I signaling.
384 These findings establish a critical role for IFI16 in antiviral innate immune response
385 to influenza virus and possibly other RNA viruses (a proposed signaling model is
386 depicted in Extended Data Fig. 8).

387 We found that IFI16 was strongly induced by IAV, which is consistent with
388 previous findings that IFI16 could be induced by RNA viruses infection and be
389 upregulated by the type I and type III interferons as an ISG²⁷⁻²⁹. IFI16 is known to
390 boost sensing of intracellular DNA and subsequent IFN-I induction^{21,24,26}; it functions
391 as a cytoplasmic immune sensor-mediating pyroptotic death of tissue CD⁴⁺ T cells
392 abortively infected with HIV-1²². Thus, the main role of IFI16 had been assumed to be
393 a cytoplasmic sensor of viral DNA⁴³. However, this is at odds with the findings that
394 IFI16 is predominantly localized in the nucleus³⁶. We found that IFI16 is induced in
395 the nucleus and acts as a positive transcriptional regulator of *RIG-I* during IAV
396 infection. These results confirm previous findings that IFI16 regulates RNA

397 virus-mediated IFN-I responses as a transcriptional factor²⁷. We also found that IFI16
398 was induced in the cytoplasm, sensed and interacted with influenza viral RNAs,
399 which is consistent with recent findings that IFI16 directly binds to incoming
400 Chikungunya virus genome RNA and acts as a PRR³⁰. Overexpression of IFI16 in
401 cells significantly increased IFN- β expression and reduced in viral titers, whereas
402 knockdown or knockout of *IFI16* had the opposite effects, suggesting IFI16 is an
403 important antiviral factor in IAV infection. Therefore we demonstrate an important
404 mechanism of IFI16 in RLR-mediated antiviral innate immune response to influenza
405 virus and further our understanding of the role of IFI16 in innate immunity.

406 Viral RNA sensor RIG-I is thought to be the most important sensor of influenza
407 virus infection⁹ in the recognition of cytoplasmic dsRNA leading to the transcriptional
408 activation of IFN-I and downstream ISGs¹⁴. Thus, identification of positive regulators
409 of RIG-I could be important in the control of virus infection. DNA-dependent
410 activator of IFN-regulatory factor (DAI), a cytosolic DNA sensor, has already been
411 found to recognize genomic RNA and regulate virus-induced cell-death pathways and
412 thereby plays an important role in the pathogenesis of IAV infection^{44,45}. Here, we
413 demonstrated that IFI16 binds to viral RNAs and enhances RIG-I-mediated
414 production of IFN-I during IAV infection. We further identified that IFI16 interacted
415 with RIG-I that involves the PYRIN domain of IFI16. An interaction of IFI16 with
416 RIG-I as a complex via siRNA was previously reported⁴⁶. Notably, we found that
417 IFI16 facilitates RIG-I binding to IAV vRNAs during infection and promotes
418 virus-induced K63-linked polyubiquitination of RIG-I, indicating that IFI16 positively

419 contributes to RIG-I-dependent antiviral responses. Presently, it is not clear if the
420 filamentous structures of IFI16 are necessary for IFI16-vRNAs and IFI16-RIG-I
421 interactions, or about the types of viral RNA structures that are needed to interact with
422 IFI16.

423 Collectively, our study shows that IFI16 induced by influenza virus infection
424 positively regulates the RIG-I signaling by enhancing its transcriptional expression
425 through recruitment of RNA Pol II to the RIG-I promoter, and sensing of viral RNA to
426 promote virus-induced K63-linked polyubiquitination of RIG-I. This study highlights
427 an important mechanism of IFI16 in RLR-mediated innate antiviral immune response
428 to IAV and possibly other RNA viruses infection, and expands our understanding of
429 the functions of the innate immune system in intracellular virus recognition which
430 could help to develop new strategies to modulate antiviral responses.

431

432

433

434

435

436

437

438

439

440

441 **Materials and Methods**

442 **Ethics statement**

443 All animal experiments were performed in accordance with institutional
444 guidelines of China Agricultural University (CAU) (approval SKLAB-B-2010-003)
445 and approved by the Beijing Association for Science and Technology of China
446 (approval SYXK, Beijing, 2007-0023).

447 **Cells**

448 Madin-Darby canine kidney cells (MDCK), human embryonic kidney cells
449 (HEK293), and human lung adenocarcinoma epithelial cells (A549) were maintained
450 in-house. THP-1 cell line was kindly provided by Dr. Shijun Zheng (China
451 Agricultural University). *IFI16*^{-/-} A549 and *RIG-I*^{-/-} HEK293 cell lines were
452 generously given by Dr. Yu Chen (Sun Yat-sen University) and Dr. Wenjun Liu
453 (Institute of Microbiology, Chinese Academy of Sciences), respectively. *Ifnar1*^{-/-} A549
454 cell line was generously given by Dr. Ying Zhu (Wuhan University). And
455 2fTGH-ISRE cell line was kindly provided by Dr. Fuping You (Peking University)⁴⁷.
456 HEK293T-Gluc cells were kindly provided by Dr. Shan Cen (Chinese Academy of
457 Medical Sciences and Peking Union Medical School)⁴⁸. Primary bone
458 marrow-derived macrophages (BMDMs) were produced as described⁴⁹. Cells were
459 cultured in DMEM supplemented with 10% (v/v) heat-inactivated fetal bovine serum
460 (FBS; Gibco), 100 U/mL penicillin and 100 µg/mL streptomycin.

461 **Viruses**

462 Influenza A/Puerto Rico/8/1934 (PR8; H1N1) strain was maintained in our

463 laboratory. PR8-GFP virus was generated by insertion of GFP CDS sequences at the
464 carboxyl terminal of NS1 as described previously⁵⁰. The methods of cell culture, mice
465 infection, and virus titration in lung tissues were performed as previously described⁴⁹.

466 **Plasmids construction and transfection**

467 *IFI16*, *RIG-I*, *TBK1*, *TRIM25* and *MAVS* genes were amplified by PCR using
468 PR8 virus-infected THP-1 cells at 8 hours post-infection (hpi). Full-length and
469 mutated IFI16 expression constructs were generated using PRK5 containing different
470 tags or pCDNA3.1-GFP vectors by recombinase-mediated recombination. Full-length
471 RIG-I expression vectors were created using PRK5-Flag or pCDNA3.1-mCherry
472 vectors. Full promoter sequences or truncations of RIG-I were generated using
473 PGL3.0 luciferase reporter (Promega). Plasmids transfection experiments in HEK293
474 or A549 cells were performed using Lipofectamine 3000 reagents (Invitrogen).
475 *IFI16*^{+/+} or *IFI16*^{-/-} A549 cells were transfected with indicated siRNAs using
476 Lipofectamine RNAiMAX reagents (Invitrogen, Carlsbad, CA, USA).

477 ***In vivo* virus infection**

478 p204-deficient (*p204*^{-/-}) mice were kindly provided by Dr. Wei Tang (Shandong
479 University). Sex- and age-matched C57BL/6 mice were purchased from department
480 of Laboratory Animal of Charles River, Beijing. Seven-weeks-old mice were
481 inoculated intranasally with PR8 virus at a dose 50 TCID₅₀ in 50 μL of
482 phosphate-buffered saline (PBS). Body weight and survival were monitored daily
483 after infection. Lung tissue lysates were generated by homogenizing snap-frozen lung
484 tissues 2 times (20 second each time) in MEM medium, and centrifuging the lung

485 suspensions at 2000 rpm for 15 min. TCID₅₀ assays were performed on MDCK cells
486 and TCID₅₀ values were calculated as previously described⁴⁹. WT and *p204*^{-/-} mice
487 were inoculated intranasally with PR8 virus at a dose 100 TCID₅₀. The
488 bronchoalveolar fluid (BALF) was collected at 0 and 3 dpi. The BD™ CBA Mouse
489 Inflammation Kit (BD Biosciences, #552364) was used to quantitatively measure the
490 IL-6 and MCP-1 levels in BALF.

491 **Antibodies and reagents**

492 Anti-IFI16 (ab191211), anti-TBK1 (ab40676), anti-NP (ab104870), anti-TBK1
493 (ab40676), anti-Ubiquitin (linkage-specific K63) (ab271929) and anti-RNA
494 polymerase II (ab5095) antibodies were from Abcam. Anti-IFI16 (sc-8023) and
495 anti-TRIM25 (sc-166926) antibodies were from Santa Cruz. Rabbit anti-p65
496 (#10745-1-AP), anti-HA (#66006-2-Ig) and anti-RIG-I (#20566-1-AP) antibodies
497 were from Proteintech. Anti-IRF3 (YT2398) antibody was from ImmunoWay
498 Biotechnology Company. Anti-Phospho-TBK1 (Ser172; #5483); anti-Phospho-IRF3
499 (Ser396; #4947), anti-IFI16 (#14970S), anti-FLAG (#8146), anti-His (#9991)
500 anti-Myc (#2278); anti-Phospho-p65 (Ser536; #3033) antibodies were from Cell
501 Signaling Technology Inc.; Poly(I:C) (TLRL-PIC) was from InvivoGen. Recombinant
502 human interferon-gamma (IFN- γ) (HY-P7025) and C-646 (HY-13823, 10 mg) was
503 from MedChemExpress.

504 ***In vitro* transcription and biotin-labeling RNA purification**

505 Templates for T7 RNA transcription were linearized from H7N9 pSPT9 plasmids
506 coding for individual RNA segments of H7N9 virus. T7 transcription reactions were

507 carried out with T7 RNA polymerase in transcription buffer and biotin-dNTPs mix
508 according to manufacturer's instructions (Promega)⁵¹. Following DNase I treatment,
509 biotin-labeled vRNAs were extracted with phenol/chloroform, ethanol precipitated
510 and purified with RNaseasy columns (Aidlab Biotechnologies) and analyzed on
511 denaturing agarose gels for correct size.

512 **Affinity purification coupled with mass spectrometry (AP-MS)**

513 THP-1 cells were treated with phorbolmyristateacetate (PMA) for 12 h, and
514 infected with H7N9 virus (at 1 MOI). After 12 h infection, cells were lysed with lysis
515 buffer and incubated with *in vitro* transcribed 2 pM biotin-labeled viral RNAs for 4 h
516 followed by incubation with pre-washed Dynabeads M-280 Streptavidin (Sigma) for 3
517 h at 4°C. Beads were washed five times with NT2 buffer (50 mM Tris-HCl pH 7.0,
518 150 mM NaCl, 1 mM MgCl₂, 0.05% NP-40); protein complex bound to the beads was
519 then boiled with 20 μL PBS at 100°C for 10 min. Pulled-down proteins were
520 identified by LC-MS.

521 **Western blotting**

522 Western blotting was performed as previously described⁴⁹. Briefly, protein
523 samples were mixed with loading buffer supplemented with 10% β-mercaptoethanol,
524 heated at 95°C for 5 min, and separated on a 10% SDS-PAGE under reducing
525 conditions. After electrophoresis, protein samples were electroblotted onto
526 polyvinylidene difluoride (PVDF) membranes (BioRad), and blocked for 2 h in
527 Tris-buffered saline (10 mM Tris-HCl, pH 8.0, containing 150 mM NaCl) containing
528 5% (w/v) non-fat dry milk and 0.5% (v/v) Tween-20. The blots were incubated with

529 the primary antibodies overnight at 4°C. The next day, the blots were incubated with
530 corresponding horseradish peroxidase (HRP)-conjugated secondary antibodies for 1 h
531 at room temperature (RT). HRP antibody binding was detected using a standard
532 enhanced chemiluminescence (ECL) kit (Thermo Scientific).

533 **Quantitative real-time RT-PCR (RT-qPCR)**

534 Total RNA from virus-infected cells or lung tissues was extracted using an RNA
535 isolation kit (Thermo Scientific). First-strand cDNA was synthesized from 1 µg of
536 total RNA using TransScript RT reagent Kit (TransGen). Uni-12 primer was used for
537 the detection of influenza viral RNA and oligo dT and random primers were used for
538 detecting host and viral genes. Generated cDNA was subjected to qPCR in a 25 µL
539 reaction volume using FastStart Universal SYBR Green Master mix (Roche, China).
540 Human *β-actin* and mouse *GAPDH* genes were amplified for normalization of the
541 cDNA amount used in qPCR. Reactions were conducted in triplicates, and the data
542 were analyzed using the $2^{-\Delta\Delta C_t}$ method. qPCR primers used in this study are listed in
543 Table S1.

544 **Type I Interferons bioassay**

545 During PR8 virus infection, IFN-I released in human cell culture media was
546 quantified in 2fTGH-ISRE cells as previously described⁵². In brief, 200 µL of cell
547 culture supernatants were incubated with confluent 2fGTH-ISRE-Luci cells in
548 24-well plate for 6 h. Cells were then lysed in passive lysis buffer and subjected to
549 luciferase quantification (Promega). A serial dilution of recombinant human IFN-β
550 (Invitrogen) was used as reference.

551 **Luciferase reporter assays**

552 HEK293 cells seeded on 24-well plates were co-transfected with 125 ng of the
553 luciferase reporter plasmids and equal amount of various expression plasmids or
554 empty controls. Ten ng of pRL-TK plasmids were used as an internal control. After 24
555 h of transfection, Rluc and Fluc expression were measured in the presence or absence
556 of virus stimulation for 12 h using the Dual-Luciferase Reporter Assay kit (Promega)
557 in a TD-20/20 Luminometer according to the manufacturers' recommendations.
558 Results were normalized to corresponding control reporter constructs.

559 Gaussia Luciferase reporter assays were performed according to standard
560 procedures described in detail elsewhere⁴⁸. Briefly, HEK293T-Gluc cells were
561 transfected with either *IFI16*-Flag or Flag control plasmids, followed by infection
562 with PR8 virus (MOI = 1) for 24 h, and viral infectivity was evaluated by the Gluc
563 activity. After a further incubation of 24 h, cell supernatants were collected and
564 measured for Gluc activity. Dimethyl sulfoxide (DMSO) was used as negative
565 controls. The inhibition rate of the tested compounds was calculated with the
566 following equation, where RLU indicates relative light unit:

567
$$\text{Inhibition rate} = (\text{RLU}_{\text{infected cells}} - \text{RLU}_{\text{tested compound}}) / (\text{RLU}_{\text{infected cells}} -$$

568
$$\text{RLU}_{\text{mock-infected cells}}) 100\%$$

569 **Histology**

570 WT and *p204*^{-/-} mice were euthanized and sacrificed at the indicated time points
571 after PR8 virus infection. Lung tissues were harvested and fixed with 4%
572 formaldehyde, followed by paraffin embedding. For histopathological analysis, 5-

573 7- μ m sections were sectioned longitudinally through the left and right lung and
574 stained using a standard hematoxylin and eosin (H&E) protocol.

575 **Immunohistochemistry**

576 Lung sections were deparaffinized with xylene and rehydrated with ethanol
577 gradations and water. Endogenous peroxidase activity was blocked using 3%
578 hydrogen peroxide in methanol. PBS containing 0.05% Tween-20 was used to wash
579 lung tissue sections in between steps. Lung sections were incubated with the primary
580 anti-NP antibody (ab20343) at a 1:100 dilution or with the isotype control at the same
581 concentration at 4°C overnight in a humidified chamber. Sections were subsequently
582 incubated with the horseradish peroxidase-conjugated secondary antibody for 60 min
583 at RT. Immunodetection was performed using the Vector Elite ABC Kit (Vectastain,
584 Vector).

585 **Co-immunoprecipitation (Co-IP)**

586 For Co-IP assays, A549 cells were infected with PR8 virus at an MOI of 5. After
587 infection, cell samples were collected and lysed in 800 μ L of IP lysis buffer (Thermo
588 Scientific) containing protease and phosphatase inhibitors. A portion of each whole
589 cell lysate sample was kept to confirm protein expression levels, and 500 μ g of cell
590 lysates were used for Co-IP assays. Lysates were incubated with anti-IFI16,
591 anti-RIG-I or IgG antibodies overnight at 4°C under constant rotation, and then 40 μ L
592 of protein A/G beads (Santa Cruz) were added and incubated for 2 h at 4°C under
593 gentle rotation. The beads were then washed four times with cold lysis buffer, and
594 analyzed by SDS-PAGE and Western blotting.

595 **RNA immunoprecipitation-qPCR (RIP-qPCR)**

596 Two 10-cm² dishes (10⁷ cells per dish) of A549 cells were infected with PR8
597 virus for 12 h. Cells were lysed with RIP lysis buffer (50 mM HEPES, 150 mM KCl,
598 2 mM EDTA, 1 mM NaF, 0.5% NP40, 0.5 mM DTT, 1× protease inhibitor cocktail,
599 25 units RNasin) for 30 min at 4°C. Cell lysates were centrifuged at 12,000 rpm for
600 15 min at 4°C and the supernatants were subjected to RNA immunoprecipitation. A 50
601 μL aliquot of cell supernatant was saved as input, and the remaining samples were
602 each incubated with 5 μg anti-IFI16 antibody or IgG antibody and 40 μL protein A/G
603 beads for 10 h at 4°C under gentle shaking. After IP, the beads were pelleted and
604 washed four times with RIP wash buffer (50 mM Tris pH 7.4, 150 mM NaCl, 1 mM
605 MgCl₂, 0.05% NP40), resuspended in 250 μL of DNase digestion buffer (40 mM Tris
606 pH 8.0, 10 mM MgSO₄, 1 mM CaCl₂), and treated with 25U RNasin (Promega) and
607 2U DNase I (NEB) at 37°C for 20 min. Beads were then washed and resuspended in
608 100 μL RIP wash buffer, 10% of each sample was removed for immunoblot analysis.
609 And samples were treated with 4U proteinase K at 55°C for 30 min. The input and
610 immunoprecipitated RNAs were isolated by 1 mL of TRIzol reagent (Sigma), and
611 viral RNAs were analyzed by RT-qPCR or RNA-seq.

612 **Chromatin Immunoprecipitation-qPCR (ChIP-qPCR)**

613 Approximately 10⁷ treated cells were cross-linked with 1% formaldehyde at RT
614 for 10 min, and the cross-linking was quenched with 0.125 M glycine for 5 min. Cells
615 were then collected by centrifugation, lysed with SDS lysis buffer containing protease
616 inhibitor cocktail, and sonicated to shear the DNA. The sonicated DNA-Protein

617 complexes were incubated with anti-IFI16 (Cell Signaling Technology, #D8B5T),
618 RNA pol-II (abcam, ab5095), or control IgG (Beyotime, #A7016) antibodies. The
619 immuno complexes were collected using Protein G Dynabeads (10004d, Invitrogen).
620 The Dynabeads were washed one time with wash buffer A (20 mM Tris-HCl (pH 8.0),
621 500 mM NaCl, 2 mM EDTA, 0.1% SDS, 1% Triton X-100), one time with wash
622 buffer B (10 mM Tris-HCl (pH 8.0), 250 mM LiCl, 1 mM EDTA, 1%NP-40), and
623 three times with wash buffer C (1 mM EDTA, 10 mM Tris-HCl, pH 8.0). The beads
624 were eluted with 100 mL elution buffer (50 mM Tris-HCl (pH 8.0), 10 mM EDTA, 1%
625 SDS), followed by incubation at 65°C overnight to reverse cross-linking. The next day,
626 the DNA was purified with QIAquick PCR purification kit (Magen, D211102) and
627 analyzed using FastStart Universal SYBR Green Master mix (Roche, China).

628 **Confocal microscopy**

629 A549 or HEK293 cells on coverslips were washed twice with pre-warmed PBS
630 and fixed with 4% paraformaldehyde for 15 min at RT. Cells were subsequently
631 permeabilized with immunostaining permeabilization buffer containing Triton X-100
632 (Beyotime Biotechnology) for 10 min and blocked in QuickBlock™ Blocking Buffer
633 for 20 min at RT. Fixed cells were incubated with indicated antibodies diluted in
634 immunostaining primary antibody dilution buffer at 4°C overnight. Coverslips were
635 then washed three times with PBS and incubated with Alexa Fluor 488-conjugated
636 secondary antibodies or Alexa Fluor 555-conjugated secondary antibodies for 1 h at
637 37°C. Coverslips were finally washed three times and mounted onto microscope
638 slides with DAPI Staining Solution (Beyotime Biotechnology) for 8 min and

639 examined by confocal microscopy. Immunostained cells were visualized using the
640 Nikon Super-resolution laser scanning confocal microscope under a 100-time oil
641 objective and analyzed by the Imaris 9.2 platform.

642 ***In situ* proximity ligation assay (PLA) microscopy**

643 A DuoLink PLA kit (#DUO92105-1KT, Sigma) was used to test protein-protein
644 interactions as described in the protocol. WT or *IFI16*^{-/-} A549 cells were infected with
645 PR8 virus at 1.0 MOI for 12 h, fixed and permeabilized as described in the confocal
646 microscopy section and blocked with DuoLink blocking buffer for 30 min at 37°C.
647 Cells were incubated with corresponding primary antibodies diluted in DuoLink
648 dilution buffer. After washing, cells were incubated with species-specific PLA probes
649 (Plus and Minus) for 1 h at 37°C under hybridization conditions and in the presence
650 of 2 additional oligonucleotides to facilitate hybridization of PLA probes if they were
651 in close proximity (<40 nm). Ligase was then added and incubated for 30 min at 37°C
652 to join hybridized oligonucleotides. Amplification polymerase was added to generate
653 a concatemeric product extending from the oligonucleotide arm of the PLA probe.
654 Finally, a detection solution consisting of fluorescence-labeled oligonucleotides was
655 added, and the labeled oligonucleotides were hybridized to the concatemeric products.
656 Nuclei was stained with Duolink *in situ* mounting medium containing DAPI.

657 **Ubiquitination assay**

658 HEK293 cells were transfected with plasmids encoding *RIG-I*-Flag, *TRIM25*-His
659 with or without coexpression of *IFI16*-Myc or Myc empty vectors, and HA-Ubiquitin
660 (WT) or HA-Ubiquitin mutants (K48 or K63). After 24 h transfection, cells were

661 harvested and lysed in RIPA buffer (50 mM Tris-HCl (pH 8.0), 150 mM NaCl, 1%
662 NP-40, 0.1% SDS, and 1 mM EDTA) containing protease inhibitor cocktail and
663 10 μ M deubiquitinase inhibitor N-ethylmaleimide (NEM, Sigma). The cell extracts
664 were immunoprecipitated with anti-Flag antibody overnight at 4°C and then beads
665 were added to the samples for 1-1.5 h at 4°C. The beads were washed three times with
666 RIPA buffer and analyzed by immunoblotting with anti-HA antibody.

667 **RNA fluorescence *in situ* hybridization (RNA FISH)**

668 A549 cells were grown in 24-well slide chambers and infected with PR8 at an
669 MOI of 1. At 12 hpi, cells were fixed for 15 min in 4% PFA, then permeablized and
670 dehydrated by sequential 3 min incubations as follows: once with 70% ethanol, once
671 with 85% ethanol, and three times with 100% ethanol. Cells were then hybridized
672 with the Alexa Fluor® 488-conjugated NP RNA target probes (NP-probes,
673 GenePharma) of PR8 virus in hybridization buffer for 10 min at 75°C. Cells were
674 further incubated for 12-16 h at 37°C. Finally, cells were stained with anti-IFI16 and
675 secondary antibodies, and the nuclei was stained with DAPI as previously described.

676 **Microscale thermophoresis technology (MST)**

677 HEK293 cells were separately transfected with the *HINa*-GFP, *HINb*-GFP, and
678 *PYRIN*-GFP expression vectors. After 24 h of transfection, cell lysates were collected
679 and incubated with two-fold serial dilutions of indicated viral RNAs in
680 MST-optimized buffer at a constant concentration (20-100 nM). Equal volumes of
681 binding reactions were mixed by pipetting and incubated for 15 min at RT. Mixtures
682 were enclosed in standard-treated glass capillaries and loaded into the instrument

683 (Monolith NT.115, NanoTemper, Germany). To identify whether IFI16 directly binds
684 to the IAV RNAs, the transcribed RNAs were labeled with fluorescein RNA labeling
685 mix (#41027920, Sigma) and purified as previously described. Purified GST-IFI16
686 proteins (Abcam, ab158724) were incubated with different amounts of IAV full-length
687 fluorescein labeled RNAs, followed by MST assays. For all the measurements,
688 200-1000 counts were obtained for the fluorescence intensity. Kd values were
689 determined with the NanoTemper analysis tool.

690 **RNA pull down assay**

691 HEK293 cells were transfected with Flag-tagged *RIG-I*, *IFI16*, *TBK1* or *MAVS*
692 vectors. After 24 h transfection, cells were collected and lysed with lysis buffer (50
693 mM Tris-HCl pH 7.0, 150 mM NaCl, 1 mM MgCl₂, 0.05% NP-40). Cell lysates were
694 mixed with transcribed biotin-labeled viral NP RNA for 4 h at 4°C and incubated with
695 pre-washed Dynabeads M-280 Streptavidin (Sigma) for another 3 h at 4°C. The
696 protein samples bound to the beads were boiled and analyzed by SDS-PAGE and
697 Western blotting.

698 **DNA pull down assay**

699 IFI16 proteins were purified from *IFI16*-Flag overexpressing HEK293 cells by
700 immunoprecipitation using M2 beads (Sigma). Biotinylated mutant DNA probes were
701 synthesized by an EMSA Probe Biotin Labeling Kit (Beyotime, #GS008) and were
702 annealed and incubated with the purified Flag-tagged IFI16 proteins for 30 min in
703 binding buffer (10 mM Tris, 1 mM KCl, 1%NP-40, 1 mM EDTA, 5% glycerol) at RT.
704 Then, 40 µL prewashed Dynabeads M-280 Streptavidin (Sigma) were added for

705 incubation at 4°C for 1 h. The mutant probe-binding proteins were eluted by boiling
706 and analyzed by immunoblotting.

707 **Statistical analysis**

708 For all the bar graphs, data were shown as means ± SEM. All statistical analyses
709 were performed using GraphPad Prism software version 7.00 (GraphPad Software
710 Inc., USA). Kaplan-Meier method was employed for survival analysis. Differences in
711 means were considered statistically significant at $p < 0.05$. And significance levels are
712 as follow: * $p < 0.05$; ** $p < 0.01$; *** $p < 0.001$; NS., non-significant.

713 **Reporting Summary**

714 Further information on research design is available in the Nature Research
715 Reporting Summary linked to this article.

716 **Data Availability**

717 Mass spectrometry proteomics data have been deposited with the
718 ProteomeXchange Consortium via the PRIDE⁵³ partner repository
719 (<https://www.ebi.ac.uk/pride/>) with the dataset identifiers PXD020723 and
720 10.6019/PXD020723. The accession number for RNA-seq data: GSE157609,
721 GSE158122.

722

723

724

725

726

727 **Author contributions**

728 Z.M.J and F.H.W performed and analyzed most of experiments; Y.Y.Z, T.W, and
729 W.H.G performed affinity purification coupled with mass spectrometry analysis; S.F.Y,
730 H.L.S, J.P, Y.P.S, M.Y.W, and Q.T, generated biochemical reagents; C.J.G and K.C.C
731 guided and analyzed the data; F.H.W and J.H.L conceived and supervised the study.

732

733

734

735

736

737

738

739

740

741

742

743

744

745

746

747

748

749 **Competing interest declaration**

750 The authors declare no competing interests.

751

752

753

754

755

756

757

758

759

760

761

762

763

764

765

766

767

768

769

770

771 **Acknowledgments**

772 We thank Dr. Fuping You (Peking University), Dr. Wenjun Liu (Institute of
773 Microbiology, Chinese Academy of Sciences), Dr. Ying Zhu (Wuhan University) and
774 Dr. Yu Chen (Wuhan University) for kindly providing cell lines and Dr. Wei Tang
775 (Shandong University) for generously gifted p204 KO mice, respectively. This work
776 was supported by the National Key Research and Development Program of China (to
777 J.H.L., 2016YFD0500204) and the National Natural Science Foundation of China (to
778 F.H.W., 81960297).

779

780

781

782

783

784

785

786

787

788

789

790

791

792

793 **Figure legends**

794 **Figure 1. IFI16 is induced by IAV infection and involved in the pathogenesis of**
795 **virus infection.**

796 (A) Schematic representation of the viral RNA pull down-MS approach to identify
797 viral RNA-binding proteins in THP-1 cells. (B) Protein domain types significantly
798 enriched among the human interacting proteins with indicated vRNA baits. The
799 value range of Q value is [0,1]. The closer it is to zero, the more significant the
800 enrichment is. Domains with $Q \leq 0.05$ are defined as domains that are significantly
801 enriched in differentially genes. (C) mRNA expression levels, determined by
802 RT-qPCR, of 70 candidate viral RNA-binding proteins in THP-1 cells infected with
803 PR8 virus at 2.0 MOI. RNA samplings were taken at 0, 6, 12 and 24 hpi. (D) IFI16
804 protein expression in PR8 virus-infected (1.0 MOI) A549 cells was evaluated by
805 Western blotting at 0, 6, 12, 18 and 24 hpi. β -Actin detection used as loading control.
806 (E) Intracellular localization of IFI16 was assessed in PR8 virus-infected A549 cells at
807 0, 6, 12 and 18 hpi by confocal microscopy. Scale bars, 5 μ m. (F) Quantification of
808 intracellular localization of IFI16 in cells as in E. The data represent means \pm SD.
809 (n= 3 independent experiments). (G) A549 cells were infected with PR8 virus at 0, 12
810 and 24 hpi. Cell lysates were then immunoprecipitated with anti-IFI16. Bound
811 proteins were analyzed by immunoblots with anti-acetylated lysine. (H) A549 cells
812 were pre-incubated with C-646 for 2 h, infected with PR8 virus for 1 h, washed with
813 PBS and incubated in complete medium with or without C-646. *In situ* PLA assay
814 used to assess acetylation of IFI16 with anti-IFI16 and anti-acetylated lysine
815 antibodies on 24 hpi. Scale bars, 28.7 μ m (top) and 14.6 μ m (bottom). (B): the results
816 were assessed using a parametric paired t-test (Student's one-tailed t-test). (D) to (H):
817 Data presented are representative of three independent experiments. Statistical

818 significance in (F) was determined by unpaired two-tailed Student's t-test.

819 **Figure 2. IFI16 expression inhibits IAV infection *in vitro*.**

820 (A) A549 cells were transfected with *IFI16*-Flag plasmids or control for 24 h and then
821 infected with PR8 virus at 1.0 MOI for 18 h. Viral titers were measured by TCID₅₀
822 assay. Data presented as means ± SEMs and are representative of three independent
823 experiments. (B) A549 cells were transfected with *IFI16*-Flag plasmids or control for
824 24 h and then infected with PR8 virus at 1.0 MOI. NP and M1 proteins were detected.
825 Data were quantified and shown as the ratio of NP to β-actin and M1 to β-actin (right),
826 the data represent means ± SEMs (n = 3). (C) HEK293T-Gluc cells were transfected
827 with different amounts of *IFI16*-Flag or control, followed by infection with PR8 virus
828 (MOI = 1) for 24 h. Viral infectivity was determined. Data presented as means ±
829 SEMs and are representative of three independent experiments. (D) Viral titers in PR8
830 virus-infected (1.0 MOI) *IFI16*^{+/+} and *IFI16*^{-/-} A549 cells were measured by TCID₅₀
831 assay. Data presented as means ± SEMs and are representative of three independent
832 experiments. (E) The NP and M1 protein expression in 1 MOI of PR8 virus-infected
833 *IFI16*^{+/+} and *IFI16*^{-/-} A549 cells was analyzed. Data were quantified and shown as the
834 ratio of NP to β-actin and M1 to β-actin (right), the data represent means ± SEMs (n
835 = 3). (F) *IFI16*^{+/+} and *IFI16*^{-/-} A549 cells were transfected with *IFI16*-Flag plasmids or
836 empty control for 24 h and then infected with PR8 virus at 1.0 MOI. NP and M1
837 proteins in virus-infected A549 cells was detected. Data were quantified and shown as
838 the ratio of NP to β-actin and M1 to β-actin (right) the data represent means ± SEMs
839 (n = 3). (G) Fluorescence microscopy images of viral replication (green) in *IFI16*^{+/+}
840 and *IFI16*^{-/-} A549 cells after infection with GFP-PR8 virus for 12 h. Scale bar,
841 200 μm. (B) and (D) to (G): data are representative of three independent experiments.
842 Statistical significance in (A) to (F) was determined by unpaired two-tailed Student's

843 t-test.

844 **Figure 3. *p204*-deficient mice are susceptible to IAV infection.**

845 (A) WT and *p204*^{-/-} mice (n = 6) were infected with 50 TCID₅₀ of PR8 virus. Changes
846 in body weight were monitored daily. Data presented as means ± SD. (B) Survival of
847 WT and *p204*^{-/-} mice infected with 50 TCID₅₀ of PR8 virus. Data presented were
848 pooled from three independent experiments. Kaplan-Meier Survival Curves were
849 compared using the log-rank (Mantel-Cox) analysis. (C) Viral titers in lung tissues
850 from 50 TCID₅₀ of PR8 virus-infected WT and KO mice at 4 and 6 dpi were
851 determined by EID₅₀ assay. Data are from three independent experiments with n = 6
852 mice per group run in triplicate. Error bars indicate SEM. (D) Viral NP mRNA and
853 vRNA in lung tissues of PR8 virus-infected WT and KO mice at 3 dpi were
854 determined by RT-qPCR. Data presented as means ± SEMs and are representative of
855 three independent experiments. (E) Viral NP protein expression in lung tissue sections
856 from virus-infected WT and KO mice (n =3) mice was examined by
857 immunohistochemistry. Representative sections of one mouse out of three are shown.
858 Scale bars, 800 μm (top) and 80 μm (bottom). (F) Gross lesion of lung tissues from
859 virus-infected WT and *p204*^{-/-} mice at 3 and 5 dpi. Representative sections of one
860 mouse out of three are shown. (G) H&E staining of lung tissues from virus-infected
861 WT and *p204*^{-/-} mice at 3 dpi. Scale bars, 600 μm (left) and 120 μm (right).
862 Representative of H&E staining images from 6 mice per group of three independent
863 experiments. (H) to (I): IL-6 and MCP-1 levels in BALF from virus-infected WT and
864 KO mice (n = 4) were quantified. Data are presented as means ± SD. (J) to (N) mRNA
865 expression of *IFN-β*, *viperin*, *OAS1*, *ISG15*, and *IL-6* in BMDMs of virus-infected
866 WT and KO mice was determined by RT-PCR. Data presented as means ± SEMs and
867 are representative of three independent experiments. Statistical significance in (A), (C)

868 to (D) and (H) to (N) was determined by unpaired two-tailed Student's t-test. ns =
869 non-significant.

870 **Figure 4. IFI16 enhances RIG-I-mediated production of IFN-I during IAV**
871 **infection.**

872 (A) GO-term analysis of up-regulated host proteins in IAV-infected *IFI16*^{+/+} and
873 *IFI16*^{-/-} A549 cells. Top 10 GO-terms ordered by enrichment p-values are shown.
874 p-values as indicated in legend and indices in cells correspond to number of protein
875 groups associated to individual GO-terms in respective comparison. (B) Differential
876 expression of host genes between IAV-infected and mock conditions in *IFI16*^{+/+} (X
877 axis) and *IFI16*^{-/-} (Y axis). Proteins exhibiting significant differential response are
878 highlighted in green (ISGs) or yellow (non-ISGs). (C) to (F): Gene expression of
879 *IFN-β* (C), *RIG-I* (D), *ISG56* (E), *viperin* (F) in PR8 virus-infected *IFI16*^{+/+} and
880 *IFI16*^{-/-} A549 cells at 0, 6, and 12 hpi was determined by qPCR. (G) A549 cells were
881 transfected with *IFI16*-Flag expression vectors or empty vector for 24 h and then
882 infected with PR8 virus. IFN-I in supernatants were quantified IFN-bioassay at 2, 12,
883 18, 24 and 36 hpi from 1.0 MOI infection. (H) *IFI16*^{+/+} and *IFI16*^{-/-} A549 cells were
884 infected with PR8 virus at a 1.0 MOI. IFN-I in supernatants were then measured by
885 IFN-bioassay at 2, 12, 18, 24 and 36 hpi. (I) A549 cells were transfected with
886 *IFI16*-Flag expression vectors or empty control for 24 h and then infected with 1.0
887 MOI of PR8 virus for 0, 2, 4, 8 and 12 h. RIG-I triggered downstream signaling
888 molecules were evaluated with indicated antibodies. (J) RIG-I triggered downstream
889 signaling molecules in PR8 virus-infected *IFI16*^{+/+} and *IFI16*^{-/-} A549 cells at 0, 4, 8,
890 and 12 hpi were analyzed with indicated antibodies. (K) *IFI16*^{+/+} and *IFI16*^{-/-} A549
891 cells were infected with PR8 virus at 5.0 MOI. Nuclear localization of p-IRF3 was
892 then determined by p-IRF3 (Ser396) intracellular immunostaining for confocal

893 microscopy. Scale bar represents 10 μ m. (L) Quantification of nuclear localization of
894 p-IRF3 (Ser396).(I) to (K): Data are representative of three independent experiments.
895 (A): the results were assessed using a parametric paired t-test (Student's one-tailed
896 t-test). (C) to (H) and (L): Data presented as means \pm SD from three independent
897 experiments, and the significance of the results was assessed using a parametric
898 paired t-test (Student's two-tailed t-test). ns = non-significant

899 **Figure 5. IFI16 upregulates RIG-I expression.**

900 (A) RIG-I expression in *IFI16*-Flag overexpressing A549 cells at 0, 18, 24, and 30 h
901 post-transfection was detected by Western blotting. β -Actin detection was used as
902 loading control. (B) RIG-I mRNA expression in A549 cells transfected with
903 *IFI16*-Flag plasmids for 0, 12, 18 and 24 h was quantified by RT-qPCR. (C)
904 Luciferase activity of RIG-I reporter in HEK293 cells transfected with increasing
905 amounts of *IFI16*-Flag expression vectors for 24 h. Luciferase levels were normalized
906 to Renilla levels. Values shown are fold changes over empty vector control. (D)
907 Schematic diagram of 2000 bp promoter sequence of RIG-I gene and corresponding
908 mutants. (E) HEK293 cells were co-transfected with the RIG-I promoter mutant
909 constructs and increasing amounts of *IFI16*-Flag as indicated. Luciferase levels were
910 normalized to Renilla values. Values shown as fold change over empty vector control.
911 (F) to (G): Schematic diagram of part of the RIG-I promoter sequence and every 50
912 bp-deletion mutants, and luciferase reporter assay on the truncated mutants was
913 performed as the described in (E). (H) to (I): Schematic diagram of part of the RIG-I
914 promoter sequence and every 10 bp-deletion mutants, and luciferase reporter assay of
915 these truncated mutants was performed as the described in (E). (J) A549 cells were
916 infected with PR8 virus for 12 h followed by ChIP assay. The promoter sequence
917 binding to the IFI16 was determined by RT-qPCR. (K) *IFI16*^{+/+} and *IFI16*^{-/-} A549

918 cells were infected with PR8 virus for 0 and 12 h, followed by CHIP assay. RNA Pol II
919 recruitment to RIG-I promoter was assessed by RT-qPCR. Data presented as percent
920 input minus IgG background. (L) Luciferase activity of RIG-I promoter-luciferase
921 reporter in HEK293 cells transfected with full-length IFI16 vectors and truncated
922 mutant plasmids. Luciferase levels were normalized to Renilla values. Values shown
923 as fold change over empty vector control. (A): Data are representative of three
924 independent experiments. (B) to (L): Data presented as means \pm SD from three
925 independent experiments. Statistical significance in (B) to (C) and (E) to (L) was
926 determined by unpaired two-tailed Student's t-test. ns = non-significant.

927 **Figure 6. IFI16 binds viral RNA and associates with RIG-I protein**

928 (A) Co-localization of endogenous IFI16 (green) and viral NP RNA (red) in PR8
929 virus-infected A549 cells at 0, 6, and 12 hpi was detected by RNA FISH. Nuclei were
930 stained with DAPI (blue). Scale bars, 10 μ m. Quantification of the co-localization of
931 IFI16 and NP RNA in cells (bar plots). Means \pm SD from 3 biological samples. (B)
932 Integrated Genome Viewer representation of captured IAV genomic (negative polarity)
933 reads from Flag-immunoprecipitations of PR8-infected *RIG-I*^{-/-} cells overexpressing
934 *IFI16*-Flag (top) or *RIG-I*-Flag (bottom). Each horizontal green bar represents a single
935 150 nt read and the position where it aligns relative to an IAV gene segment. (C) PCR
936 detection of PB2 vRNAs in eluted RNA from *RIG-I*-Flag, *IFI16*-Flag and indicated
937 Flag-tagged IFI16 deletions. (D) A549 cells were infected with PR8 virus at 5.0 MOI
938 for indicated duration, followed by co-immunoprecipitation with anti-IFI16 or IgG
939 and immunoblotting analysis with anti-RIG-I antibody. (E) A549 cells were infected
940 with PR8 virus at 5.0 MOI for indicated duration, followed by
941 co-immunoprecipitation with anti-RIG-I or IgG and immunoblotting analysis with
942 anti-IFI16 antibody. (F) A549 cells were infected with 1.0 MOI of PR8 virus and then

943 analyzed by PLA with anti-IFI16 and anti-RIG-I antibodies at 0, 12 and 24 hpi. The
944 right panels are enlarged. Red point indicates IFI16 plus RIG-I complexes, green
945 point indicates the viral M1 protein. Scale bars, 60 μm (left), 10 μm (right). Data
946 presented are representative of three independent experiments.

947 **Table 1. List of primer pairs used for real-time PCR in this study.**

948

949

950

951

952

953

954

955

956

957

958

959

960

961

962

963

964

965

966

967

968 **References**

- 969 1 Collins, P. J. *et al.* Crystal structures of oseltamivir-resistant influenza virus
970 neuraminidase mutants. *Nature* **453**, 1258-1261, doi:10.1038/nature06956
971 (2008).
- 972 2 Wang, M. Z., Tai, C. Y. & Mendel, D. B. Mechanism by which mutations at
973 his274 alter sensitivity of influenza A virus N1 neuraminidase to oseltamivir
974 carboxylate and zanamivir. *Antimicrob Agents Chemother* **46**, 3809-3816,
975 doi:10.1128/aac.46.12.3809-3816.2002 (2002).
- 976 3 Deyde, V. M. *et al.* Surveillance of resistance to adamantanes among influenza
977 A(H3N2) and A(H1N1) viruses isolated worldwide. *J Infect Dis* **196**, 249-257,
978 doi:10.1086/518936 (2007).
- 979 4 Furuse, Y., Suzuki, A. & Oshitani, H. Large-scale sequence analysis of M gene
980 of influenza A viruses from different species: mechanisms for emergence and
981 spread of amantadine resistance. *Antimicrob Agents Chemother* **53**, 4457-4463,
982 doi:10.1128/AAC.00650-09 (2009).
- 983 5 Eisfeld, A. J., Neumann, G. & Kawaoka, Y. At the centre: influenza A virus
984 ribonucleoproteins. *Nat Rev Microbiol* **13**, 28-41, doi:10.1038/nrmicro3367
985 (2015).
- 986 6 Blasius, A. L. & Beutler, B. Intracellular toll-like receptors. *Immunity* **32**,
987 305-315, doi:10.1016/j.immuni.2010.03.012 (2010).
- 988 7 Takeuchi, O. & Akira, S. Innate immunity to virus infection. *Immunol Rev* **227**,
989 75-86, doi:10.1111/j.1600-065X.2008.00737.x (2009).

- 990 8 Pang, I. K. & Iwasaki, A. Inflammasomes as mediators of immunity against
991 influenza virus. *Trends Immunol* **32**, 34-41, doi:10.1016/j.it.2010.11.004
992 (2011).
- 993 9 Kato, H. *et al.* Differential roles of MDA5 and RIG-I helicases in the
994 recognition of RNA viruses. *Nature* **441**, 101-105, doi:10.1038/nature04734
995 (2006).
- 996 10 Pichlmair, A. *et al.* RIG-I-mediated antiviral responses to single-stranded RNA
997 bearing 5'-phosphates. *Science* **314**, 997-1001, doi:10.1126/science.1132998
998 (2006).
- 999 11 Gack, M. U. *et al.* TRIM25 RING-finger E3 ubiquitin ligase is essential for
1000 RIG-I-mediated antiviral activity. *Nature* **446**, 916-920,
1001 doi:10.1038/nature05732 (2007).
- 1002 12 Oshiumi, H. *et al.* The ubiquitin ligase Riplet is essential for RIG-I-dependent
1003 innate immune responses to RNA virus infection. *Cell Host Microbe* **8**,
1004 496-509, doi:10.1016/j.chom.2010.11.008 (2010).
- 1005 13 Jiang, X. *et al.* Ubiquitin-induced oligomerization of the RNA sensors RIG-I
1006 and MDA5 activates antiviral innate immune response. *Immunity* **36**, 959-973,
1007 doi:10.1016/j.immuni.2012.03.022 (2012).
- 1008 14 Loo, Y. M. & Gale, M., Jr. Immune signaling by RIG-I-like receptors.
1009 *Immunity* **34**, 680-692, doi:10.1016/j.immuni.2011.05.003 (2011).
- 1010 15 Dawson, M. J. & Trapani, J. A. The interferon-inducible autoantigen, IFI 16:
1011 localization to the nucleolus and identification of a DNA-binding domain.

1012 *Biochem Biophys Res Commun* **214**, 152-162, doi:10.1006/bbrc.1995.2269
1013 (1995).

1014 16 Orzalli, M. H., Conwell, S. E., Berrios, C., DeCaprio, J. A. & Knipe, D. M.
1015 Nuclear interferon-inducible protein 16 promotes silencing of herpesviral and
1016 transfected DNA. *Proc Natl Acad Sci U S A* **110**, E4492-4501,
1017 doi:10.1073/pnas.1316194110 (2013).

1018 17 Johnson, K. E. *et al.* IFI16 restricts HSV-1 replication by accumulating on the
1019 hsv-1 genome, repressing HSV-1 gene expression, and directly or indirectly
1020 modulating histone modifications. *PLoS Pathog* **10**, e1004503,
1021 doi:10.1371/journal.ppat.1004503 (2014).

1022 18 Almine, J. F. *et al.* IFI16 and cGAS cooperate in the activation of STING
1023 during DNA sensing in human keratinocytes. *Nat Commun* **8**, 14392,
1024 doi:10.1038/ncomms14392 (2017).

1025 19 Goubau, D., Deddouche, S. & Reis e Sousa, C. Cytosolic sensing of viruses.
1026 *Immunity* **38**, 855-869, doi:10.1016/j.immuni.2013.05.007 (2013).

1027 20 Jonsson, K. L. *et al.* IFI16 is required for DNA sensing in human macrophages
1028 by promoting production and function of cGAMP. *Nat Commun* **8**, 14391,
1029 doi:10.1038/ncomms14391 (2017).

1030 21 Kerur, N. *et al.* IFI16 acts as a nuclear pathogen sensor to induce the
1031 inflammasome in response to Kaposi Sarcoma-associated herpesvirus
1032 infection. *Cell Host Microbe* **9**, 363-375, doi:10.1016/j.chom.2011.04.008
1033 (2011).

- 1034 22 Monroe, K. M. *et al.* IFI16 DNA sensor is required for death of lymphoid CD4
1035 T cells abortively infected with HIV. *Science* **343**, 428-432,
1036 doi:10.1126/science.1243640 (2014).
- 1037 23 Orzalli, M. H. *et al.* cGAS-mediated stabilization of IFI16 promotes innate
1038 signaling during herpes simplex virus infection. *Proc Natl Acad Sci U S A* **112**,
1039 E1773-1781, doi:10.1073/pnas.1424637112 (2015).
- 1040 24 Unterholzner, L. *et al.* IFI16 is an innate immune sensor for intracellular DNA.
1041 *Nat Immunol* **11**, 997-1004, doi:10.1038/ni.1932 (2010).
- 1042 25 Ansari, M. A. *et al.* Herpesvirus Genome Recognition Induced Acetylation of
1043 Nuclear IFI16 Is Essential for Its Cytoplasmic Translocation, Inflammasome
1044 and IFN-beta Responses. *PLoS Pathog* **11**, e1005019,
1045 doi:10.1371/journal.ppat.1005019 (2015).
- 1046 26 Dunphy, G. *et al.* Non-canonical Activation of the DNA Sensing Adaptor
1047 STING by ATM and IFI16 Mediates NF-kappaB Signaling after Nuclear DNA
1048 Damage. *Mol Cell* **71**, 745-760 e745, doi:10.1016/j.molcel.2018.07.034
1049 (2018).
- 1050 27 Thompson, M. R. *et al.* Interferon gamma-inducible protein (IFI) 16
1051 transcriptionally regulates type i interferons and other interferon-stimulated
1052 genes and controls the interferon response to both DNA and RNA viruses. *J*
1053 *Biol Chem* **289**, 23568-23581, doi:10.1074/jbc.M114.554147 (2014).
- 1054 28 Cao, L. *et al.* P200 family protein IFI204 negatively regulates type I interferon
1055 responses by targeting IRF7 in nucleus. *PLoS Pathog* **15**, e1008079,

1056 doi:10.1371/journal.ppat.1008079 (2019).

1057 29 Chang, X. *et al.* IFI16 Inhibits Porcine Reproductive and Respiratory
1058 Syndrome Virus 2 Replication in a MAVS-Dependent Manner in MARC-145
1059 Cells. *Viruses* **11**, doi:10.3390/v11121160 (2019).

1060 30 Kim, B. *et al.* Discovery of Widespread Host Protein Interactions with the
1061 Pre-replicated Genome of CHIKV Using VIR-CLASP. *Mol Cell* **78**, 624-640
1062 e627, doi:10.1016/j.molcel.2020.04.013 (2020).

1063 31 Monzon-Casanova, E. *et al.* The RNA-binding protein PTBP1 is necessary for
1064 B cell selection in germinal centers. *Nat Immunol* **19**, 267-278,
1065 doi:10.1038/s41590-017-0035-5 (2018).

1066 32 Grellscheid, S. N. *et al.* Molecular design of a splicing switch responsive to
1067 the RNA binding protein Tra2beta. *Nucleic Acids Res* **39**, 8092-8104,
1068 doi:10.1093/nar/gkr495 (2011).

1069 33 Li, H. *et al.* RNA Helicase DDX5 Inhibits Reprogramming to Pluripotency by
1070 miRNA-Based Repression of RYBP and its PRC1-Dependent and
1071 -Independent Functions. *Cell Stem Cell* **20**, 462-477 e466,
1072 doi:10.1016/j.stem.2016.12.002 (2017).

1073 34 Herdy, B. *et al.* Analysis of NRAS RNA G-quadruplex binding proteins
1074 reveals DDX3X as a novel interactor of cellular G-quadruplex containing
1075 transcripts. *Nucleic Acids Res* **46**, 11592-11604, doi:10.1093/nar/gky861
1076 (2018).

1077 35 Di Giammartino, D. C. *et al.* RBBP6 isoforms regulate the human

1078 polyadenylation machinery and modulate expression of mRNAs with AU-rich
1079 3' UTRs. *Genes Dev* **28**, 2248-2260, doi:10.1101/gad.245787.114 (2014).

1080 36 Li, T., Diner, B. A., Chen, J. & Cristea, I. M. Acetylation modulates cellular
1081 distribution and DNA sensing ability of interferon-inducible protein IFI16.
1082 *Proc Natl Acad Sci U S A* **109**, 10558-10563, doi:10.1073/pnas.1203447109
1083 (2012).

1084 37 Baum, A., Sachidanandam, R. & Garcia-Sastre, A. Preference of RIG-I for
1085 short viral RNA molecules in infected cells revealed by next-generation
1086 sequencing. *Proc Natl Acad Sci U S A* **107**, 16303-16308,
1087 doi:10.1073/pnas.1005077107 (2010).

1088 38 Jakobsen, M. R. & Paludan, S. R. IFI16: At the interphase between innate
1089 DNA sensing and genome regulation. *Cytokine Growth Factor Rev* **25**,
1090 649-655, doi:10.1016/j.cytogfr.2014.06.004 (2014).

1091 39 Li, D. *et al.* STING-Mediated IFI16 Degradation Negatively Controls Type I
1092 Interferon Production. *Cell Rep* **29**, 1249-1260 e1244,
1093 doi:10.1016/j.celrep.2019.09.069 (2019).

1094 40 Merkl, P. E. & Knipe, D. M. Role for a Filamentous Nuclear Assembly of
1095 IFI16, DNA, and Host Factors in Restriction of Herpesviral Infection. *mBio* **10**,
1096 doi:10.1128/mBio.02621-18 (2019).

1097 41 Antiochos, B., Matyszewski, M., Sohn, J., Casciola-Rosen, L. & Rosen, A.
1098 IFI16 filament formation in salivary epithelial cells shapes the anti-IFI16
1099 immune response in Sjogren's syndrome. *JCI Insight* **3**,

1100 doi:10.1172/jci.insight.120179 (2018).

1101 42 Morrone, S. R. *et al.* Cooperative assembly of IFI16 filaments on dsDNA
1102 provides insights into host defense strategy. *Proc Natl Acad Sci U S A* **111**,
1103 E62-71, doi:10.1073/pnas.1313577111 (2014).

1104 43 Hotter, D. *et al.* IFI16 Targets the Transcription Factor Sp1 to Suppress HIV-1
1105 Transcription and Latency Reactivation. *Cell Host Microbe* **25**, 858-872 e813,
1106 doi:10.1016/j.chom.2019.05.002 (2019).

1107 44 Thapa, R. J. *et al.* DAI Senses Influenza A Virus Genomic RNA and Activates
1108 RIPK3-Dependent Cell Death. *Cell Host Microbe* **20**, 674-681,
1109 doi:10.1016/j.chom.2016.09.014 (2016).

1110 45 Kuriakose, T. *et al.* ZBP1/DAI is an innate sensor of influenza virus triggering
1111 the NLRP3 inflammasome and programmed cell death pathways. *Sci Immunol*
1112 **1**, doi:10.1126/sciimmunol.aag2045 (2016).

1113 46 Sui, H., Zhou, M., Chen, Q., Lane, H. C. & Imamichi, T. siRNA enhances
1114 DNA-mediated interferon lambda-1 response through crosstalk between RIG-I
1115 and IFI16 signalling pathway. *Nucleic Acids Res* **42**, 583-598,
1116 doi:10.1093/nar/gkt844 (2014).

1117 47 Cao, L. *et al.* The Nuclear Matrix Protein SAFA Surveils Viral RNA and
1118 Facilitates Immunity by Activating Antiviral Enhancers and Super-enhancers.
1119 *Cell Host Microbe* **26**, 369-384 e368, doi:10.1016/j.chom.2019.08.010 (2019).

1120 48 Gao, Q. *et al.* A cell-based high-throughput approach to identify inhibitors of
1121 influenza A virus. *Acta Pharm Sin B* **4**, 301-306,

1122 doi:10.1016/j.apsb.2014.06.005 (2014).

1123 49 Wei, F. *et al.* Induction of PGRN by influenza virus inhibits the antiviral
1124 immune responses through downregulation of type I interferons signaling.
1125 *PLoS Pathog* **15**, e1008062, doi:10.1371/journal.ppat.1008062 (2019).

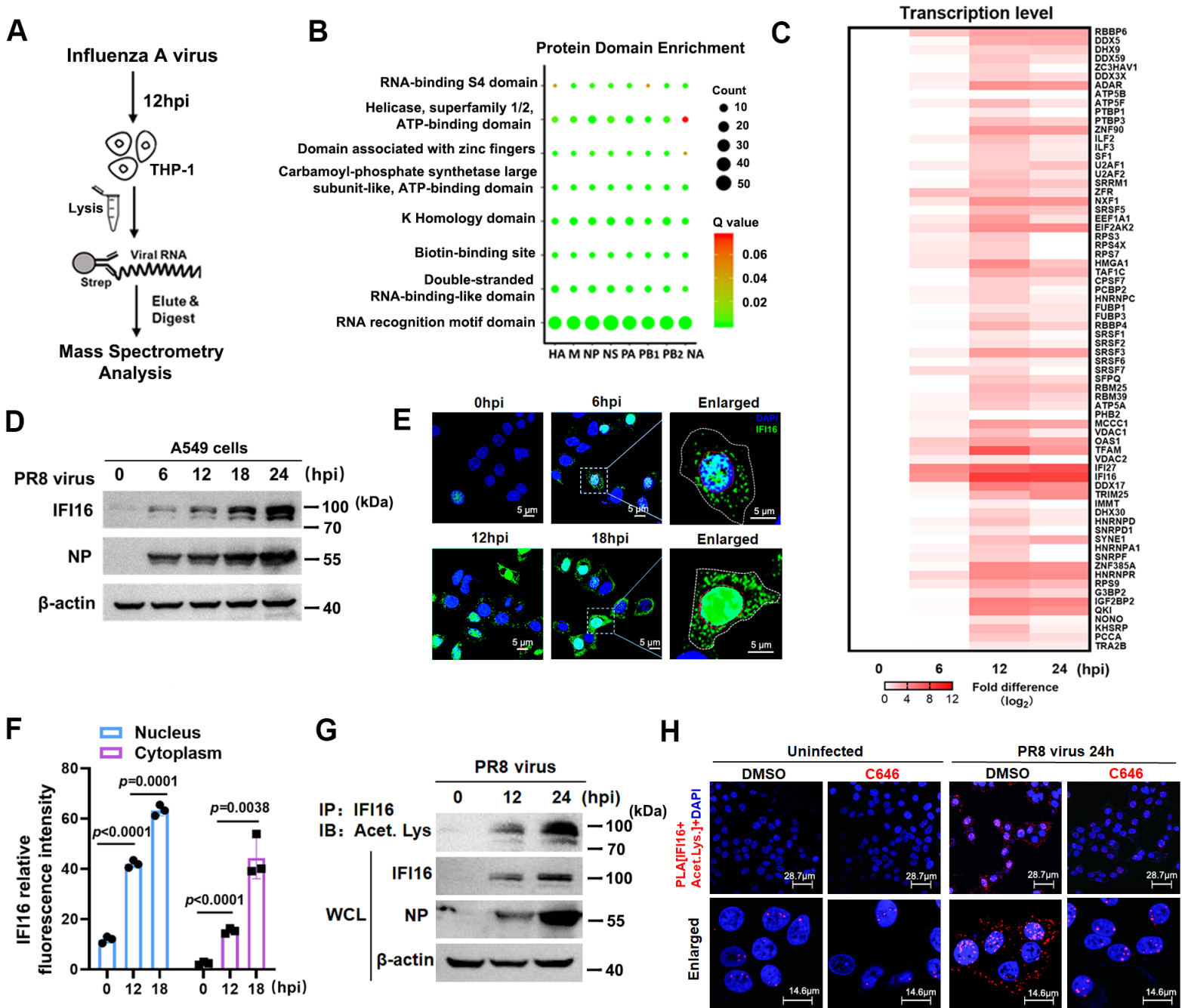
1126 50 Manicassamy, B. *et al.* Analysis of in vivo dynamics of influenza virus
1127 infection in mice using a GFP reporter virus. *Proc Natl Acad Sci U S A* **107**,
1128 11531-11536, doi:10.1073/pnas.0914994107 (2010).

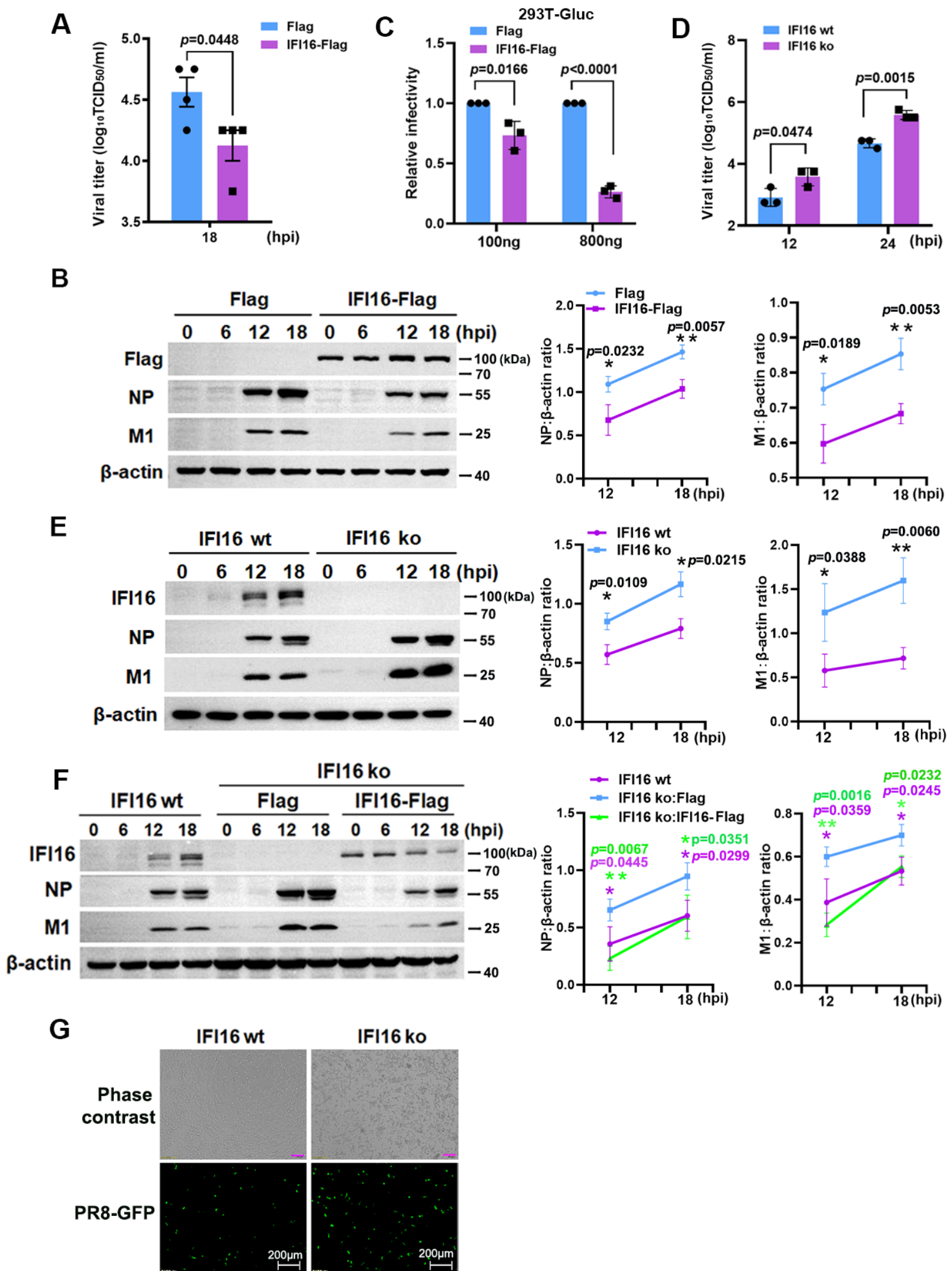
1129 51 Gavazzi, C. *et al.* An in vitro network of intermolecular interactions between
1130 viral RNA segments of an avian H5N2 influenza A virus: comparison with a
1131 human H3N2 virus. *Nucleic Acids Res* **41**, 1241-1254,
1132 doi:10.1093/nar/gks1181 (2013).

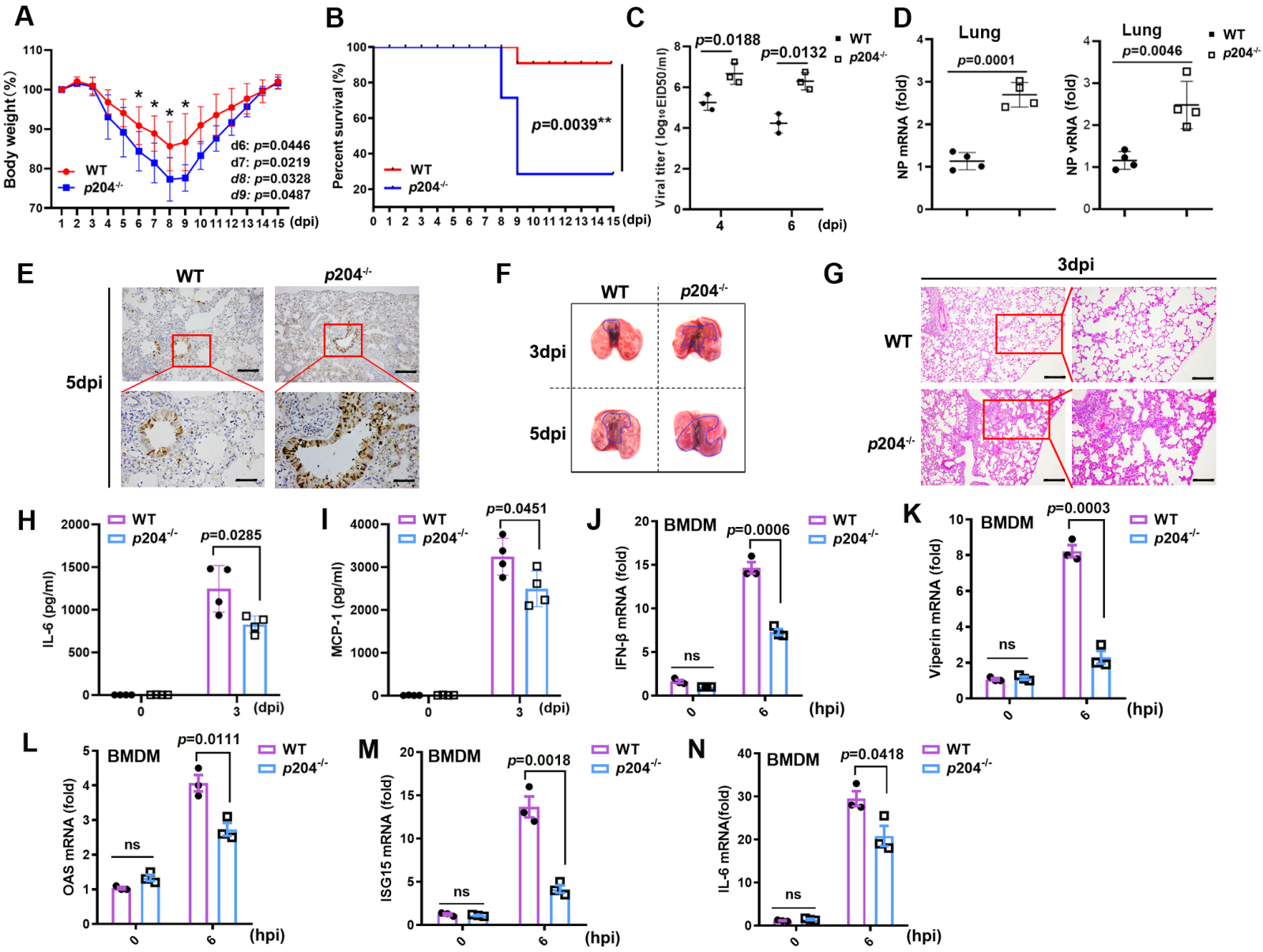
1133 52 You, F. *et al.* ELF4 is critical for induction of type I interferon and the host
1134 antiviral response. *Nat Immunol* **14**, 1237-1246, doi:10.1038/ni.2756 (2013).

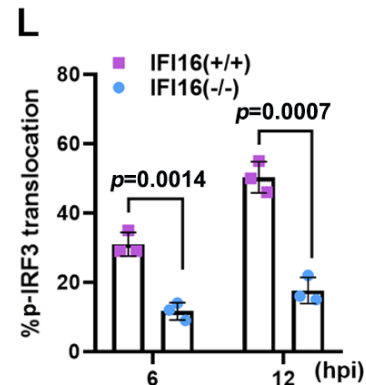
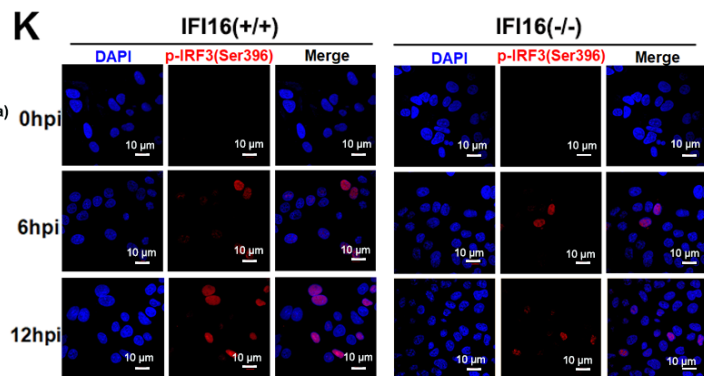
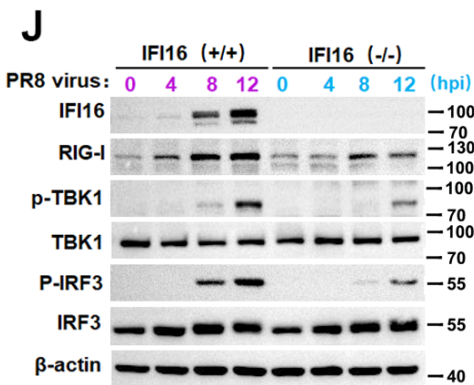
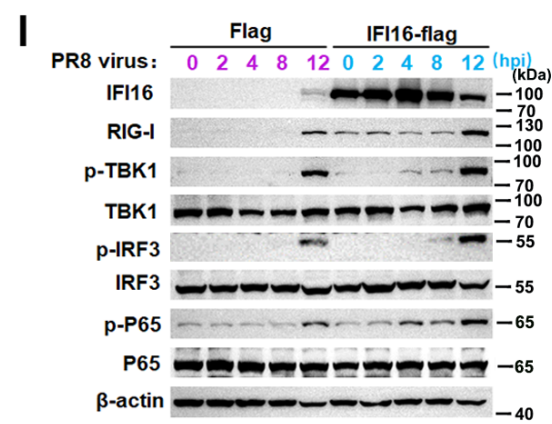
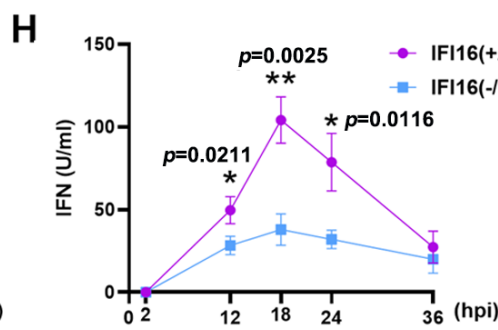
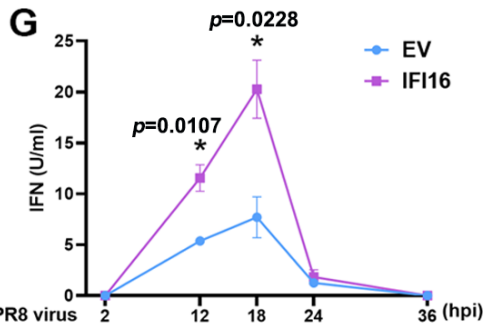
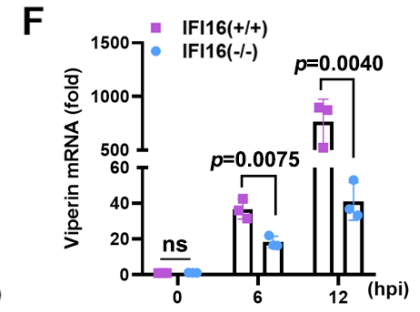
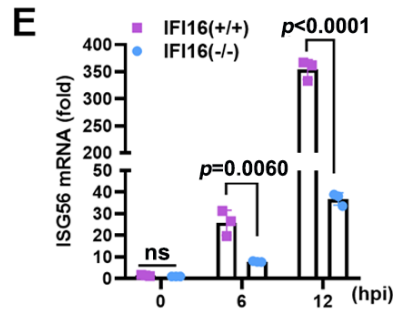
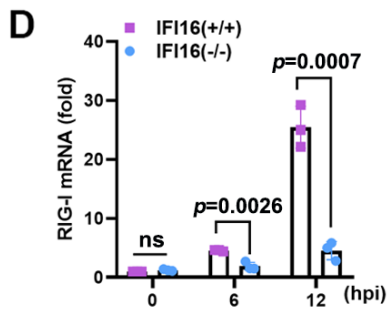
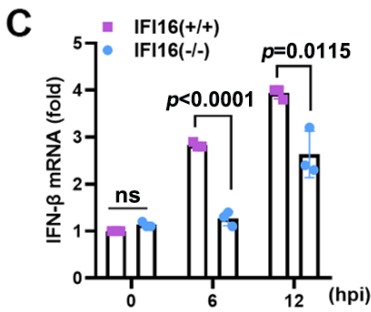
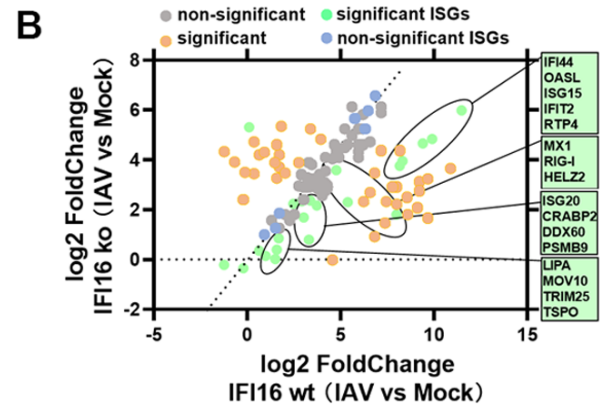
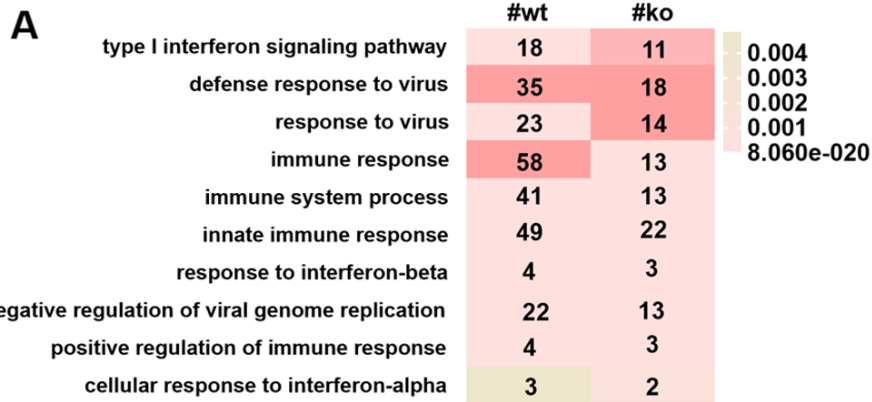
1135 53 Perez-Riverol, Y. *et al.* The PRIDE database and related tools and resources in
1136 2019: improving support for quantification data. *Nucleic Acids Res* **47**,
1137 D442-D450, doi:10.1093/nar/gky1106 (2019).

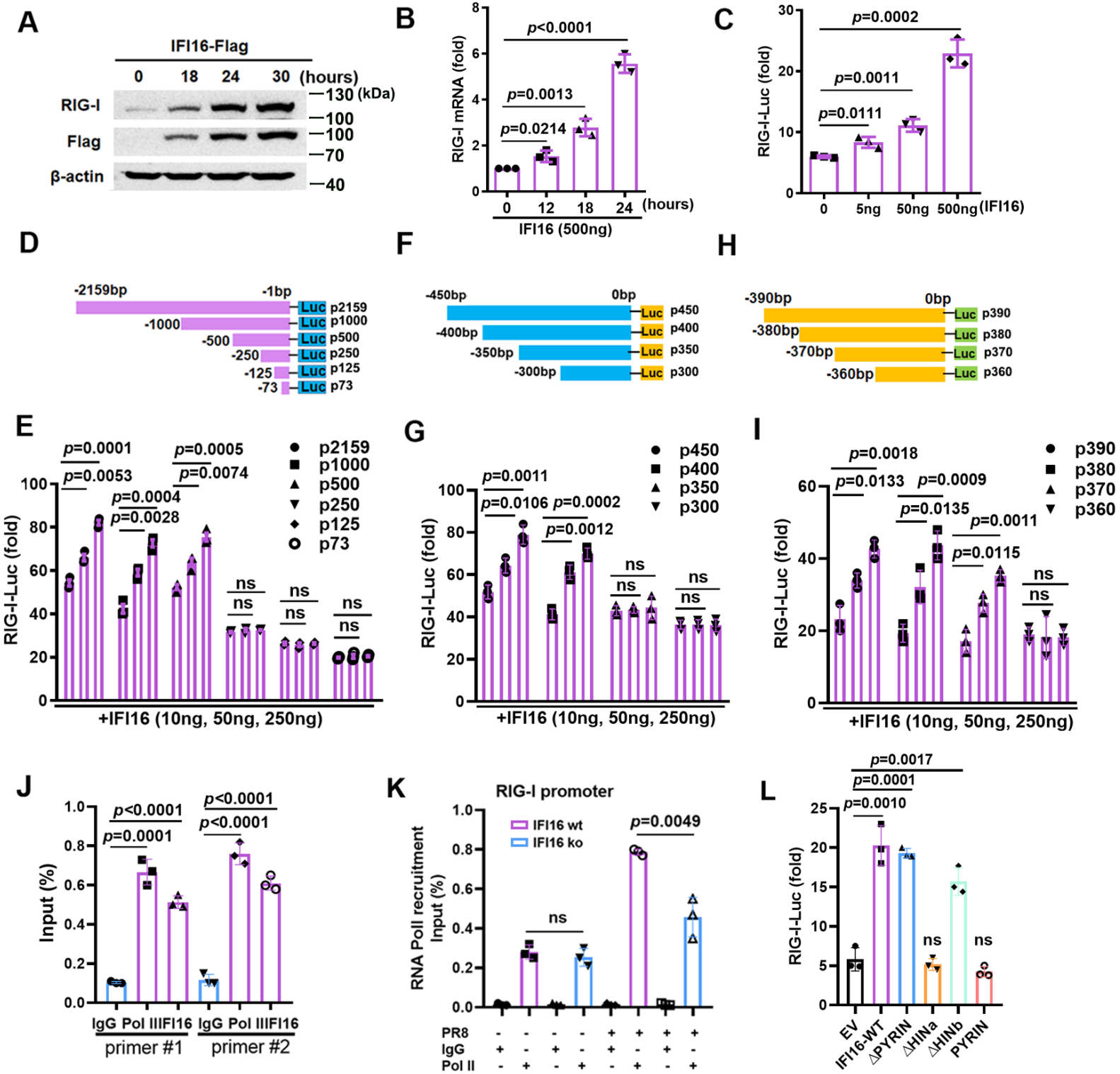
1138

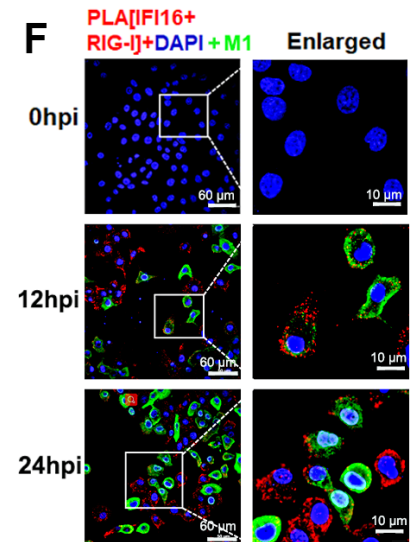
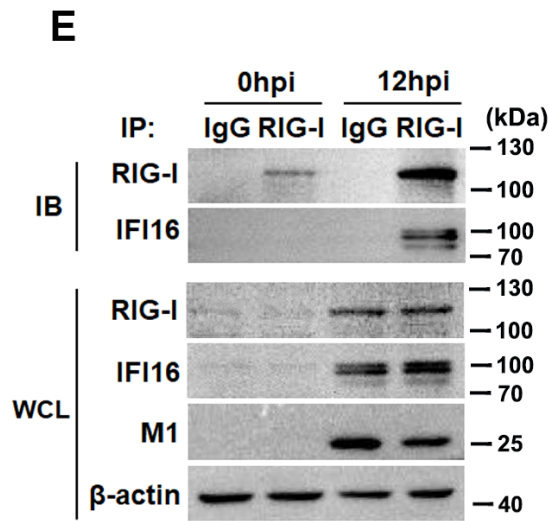
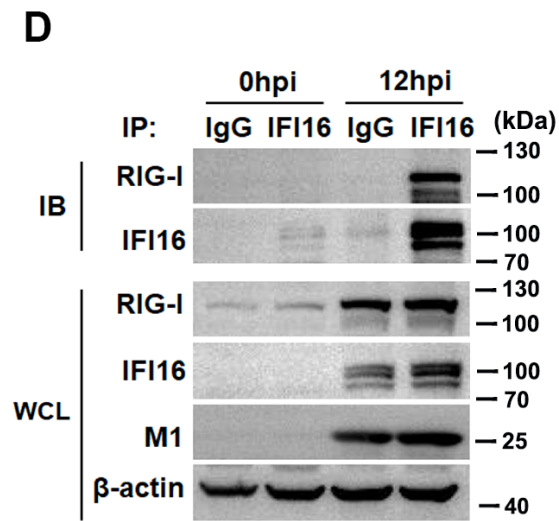
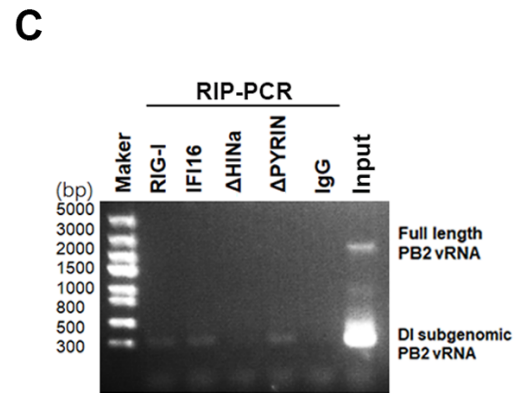
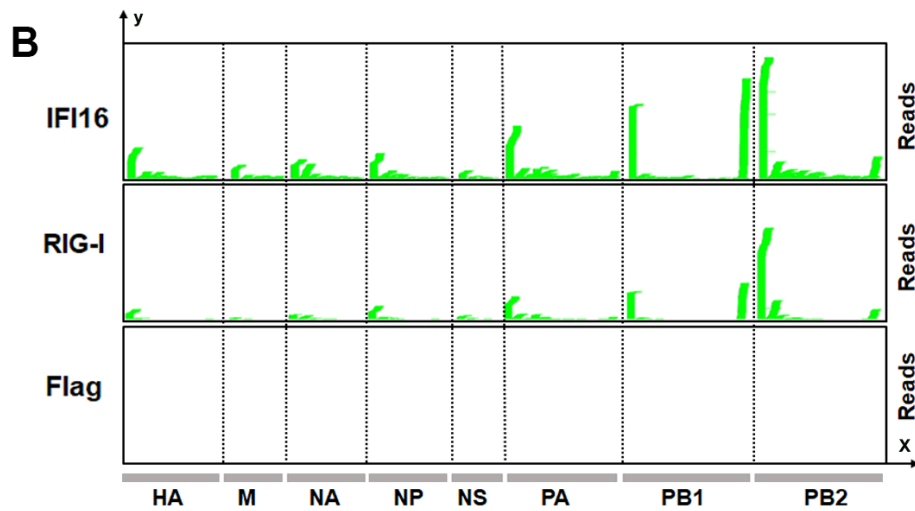
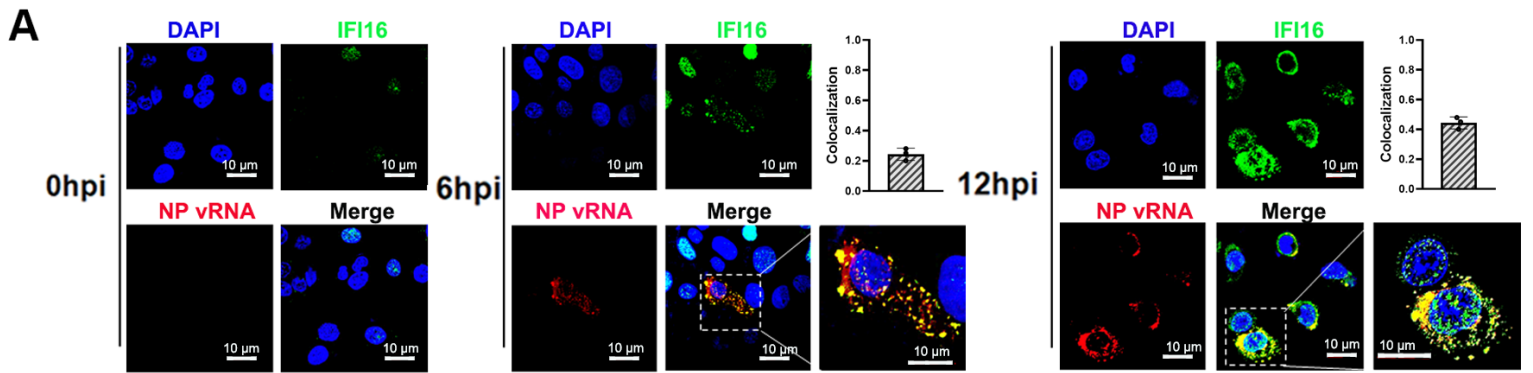


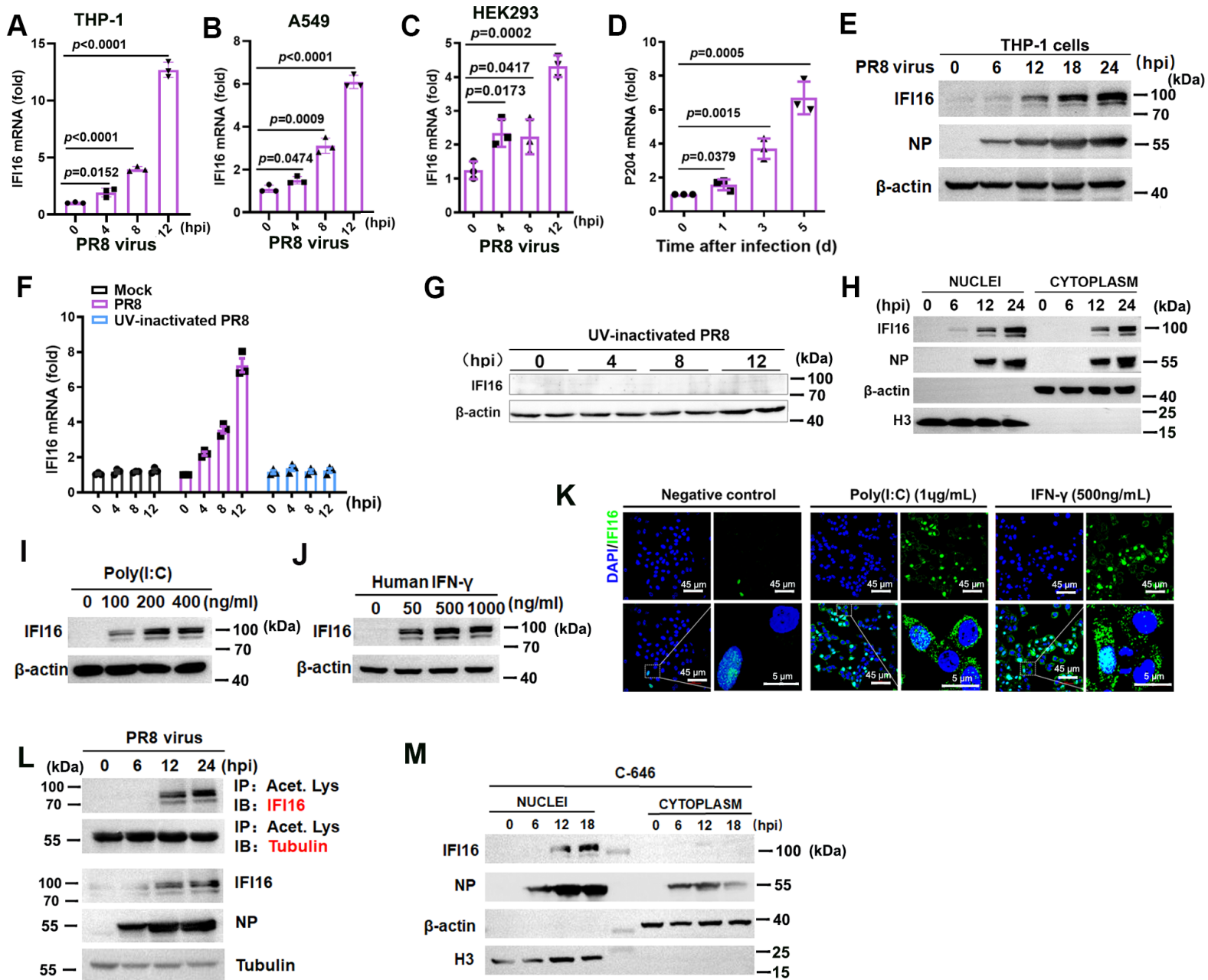


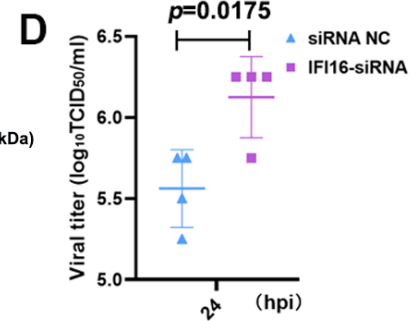
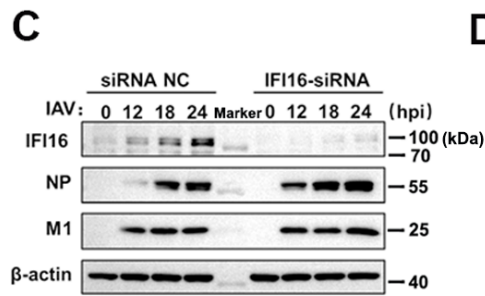
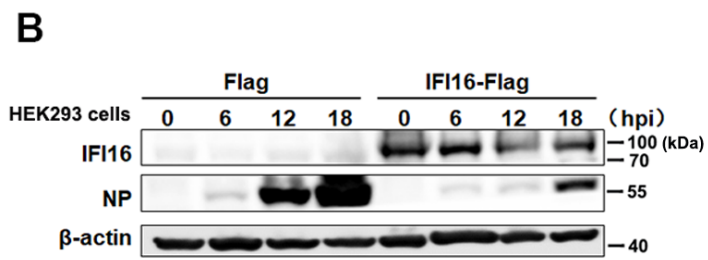
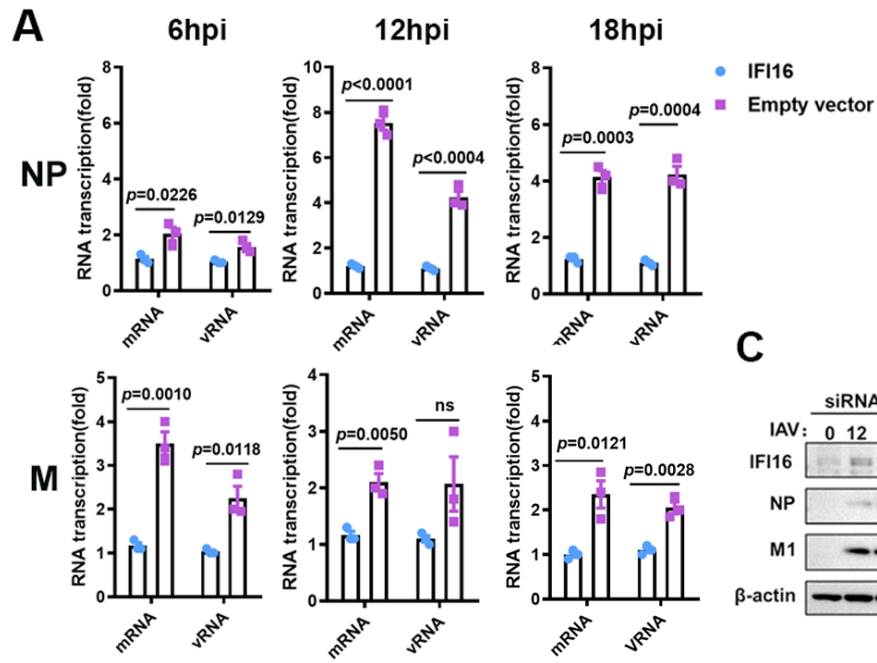


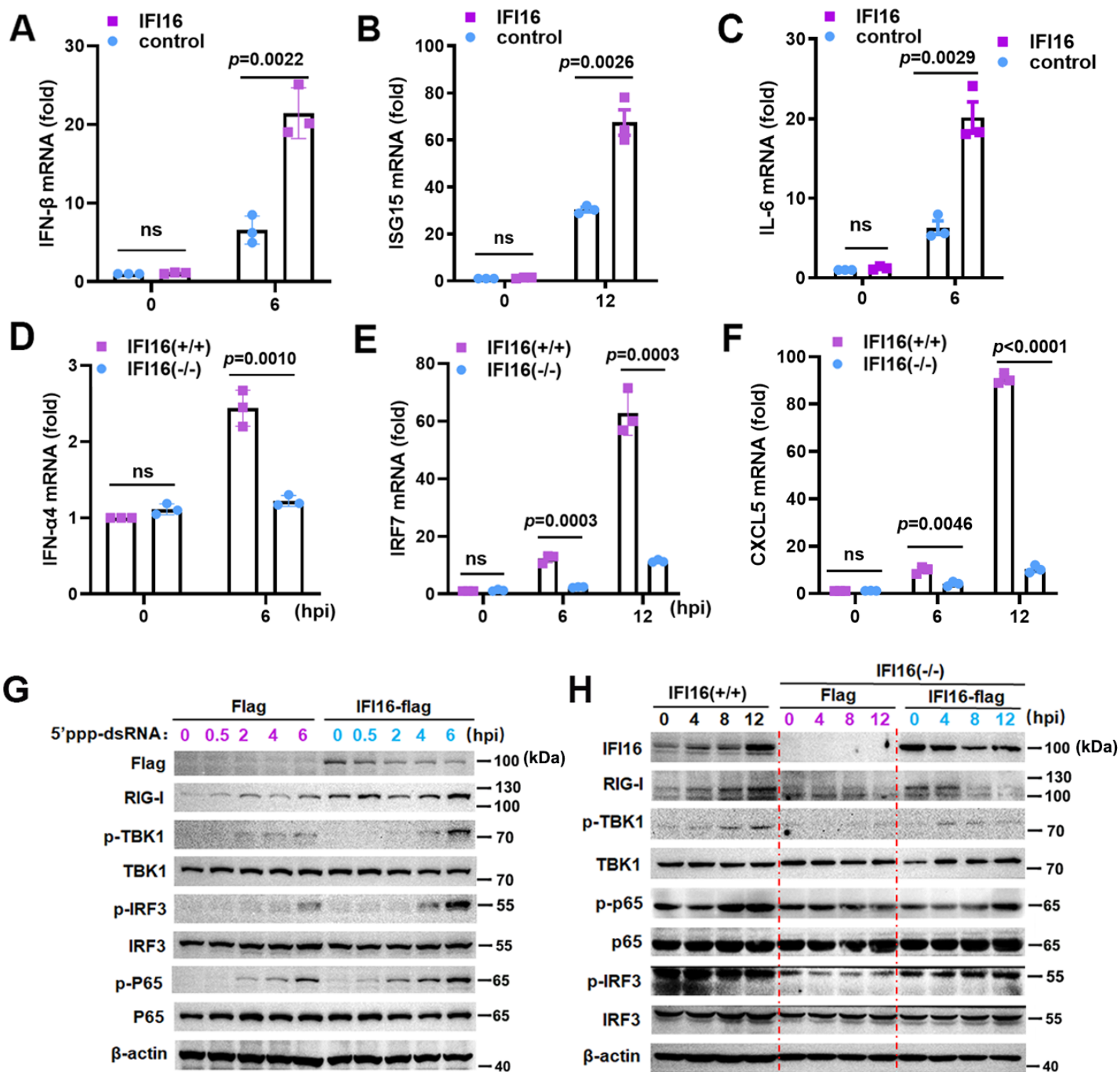


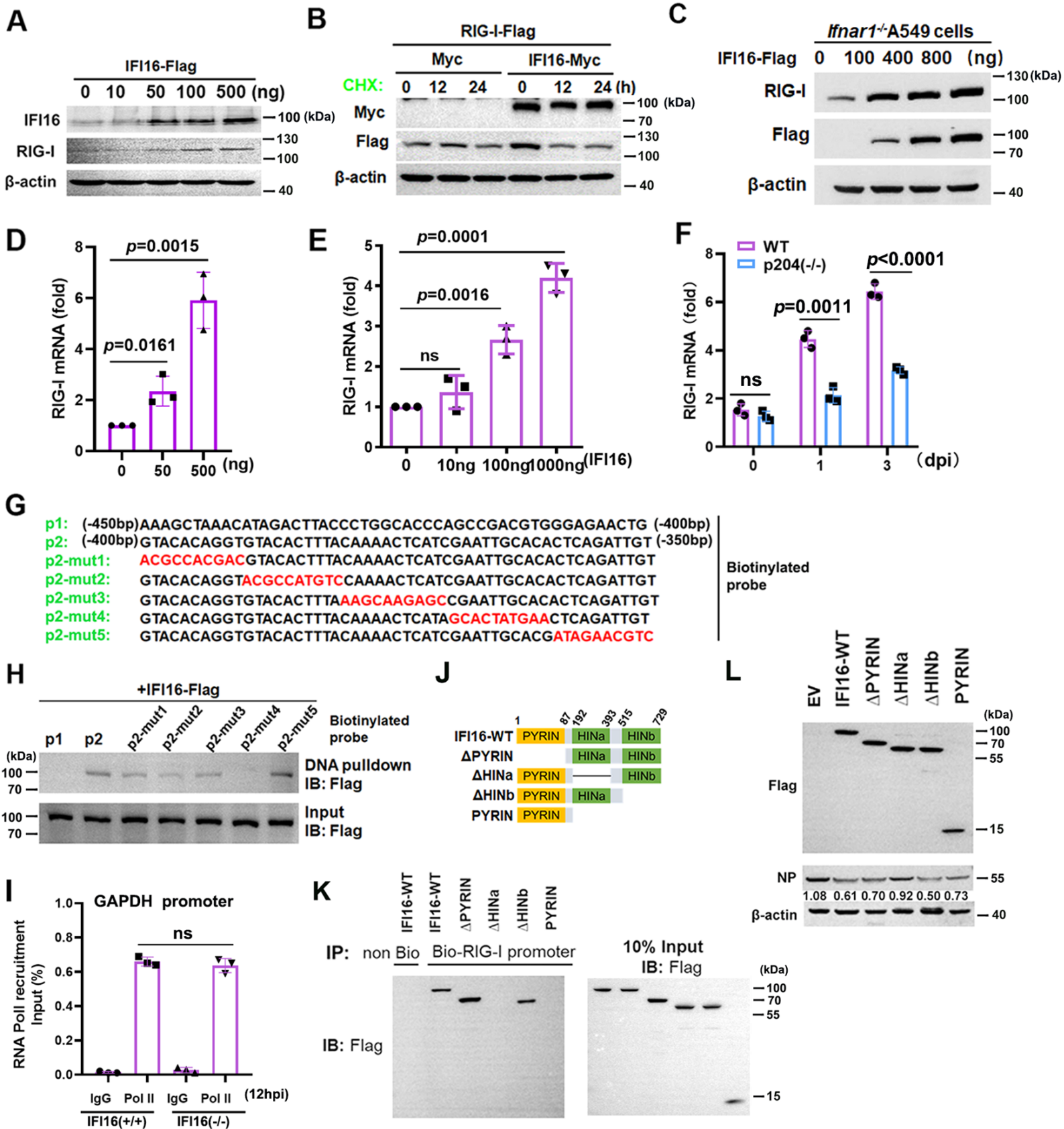


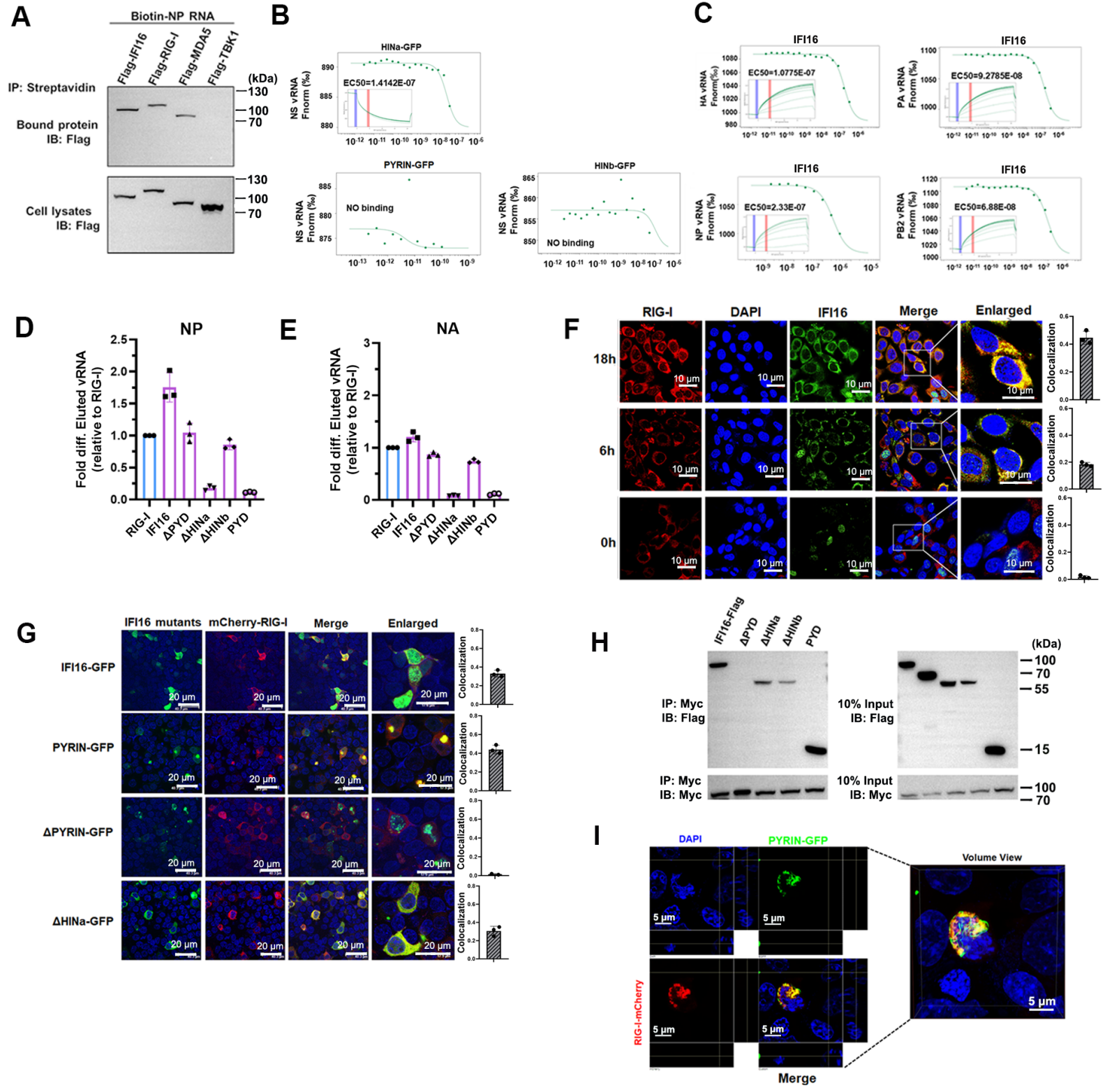


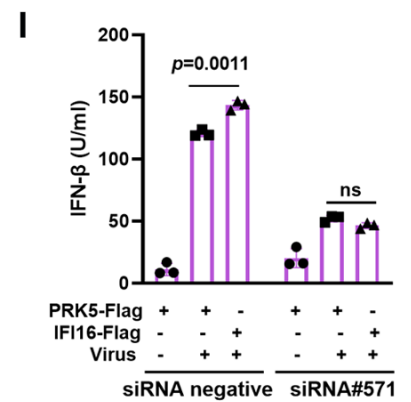
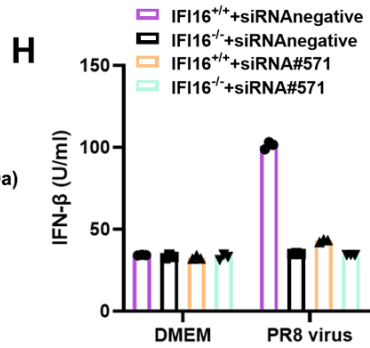
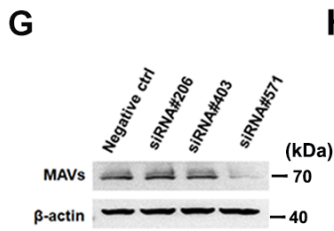
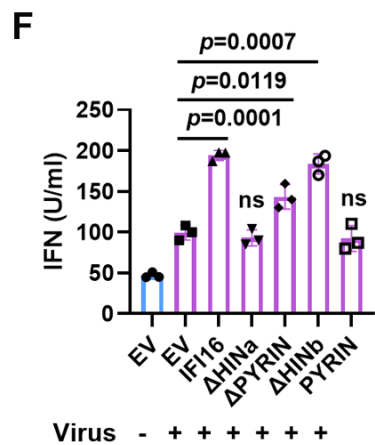
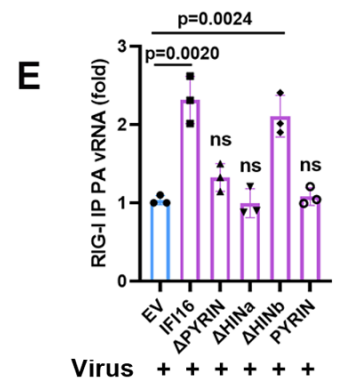
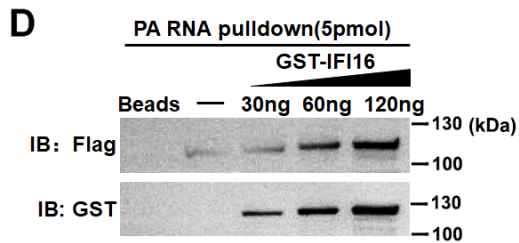
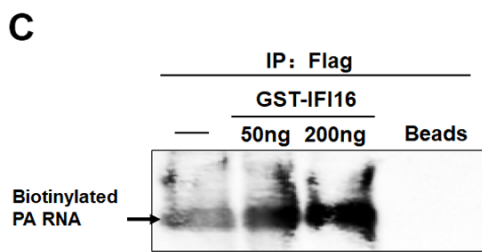
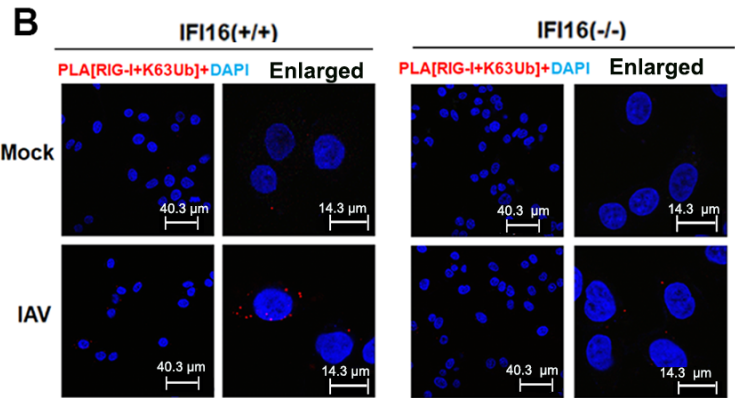
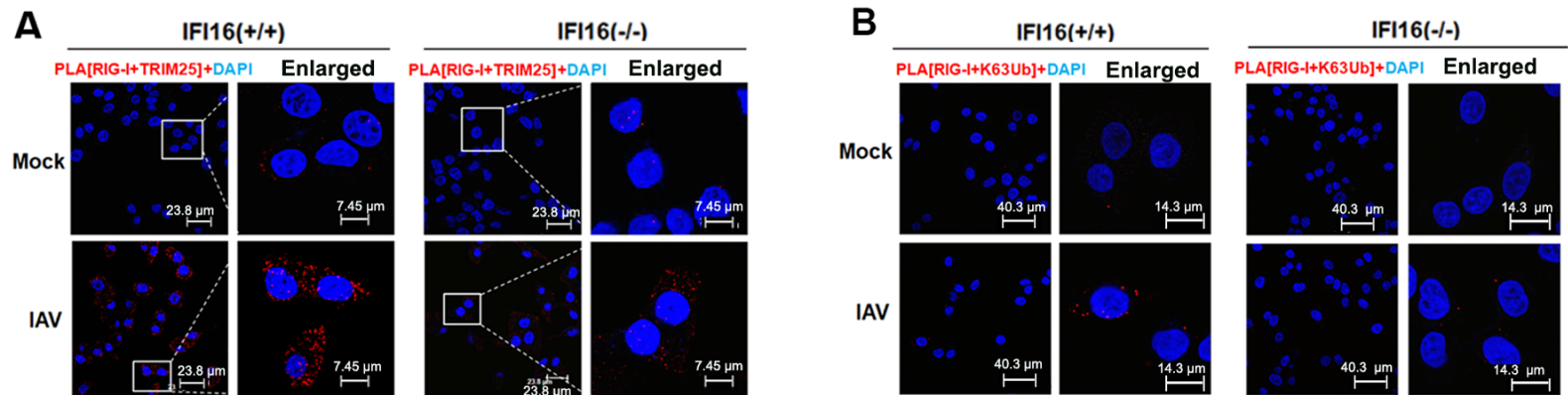


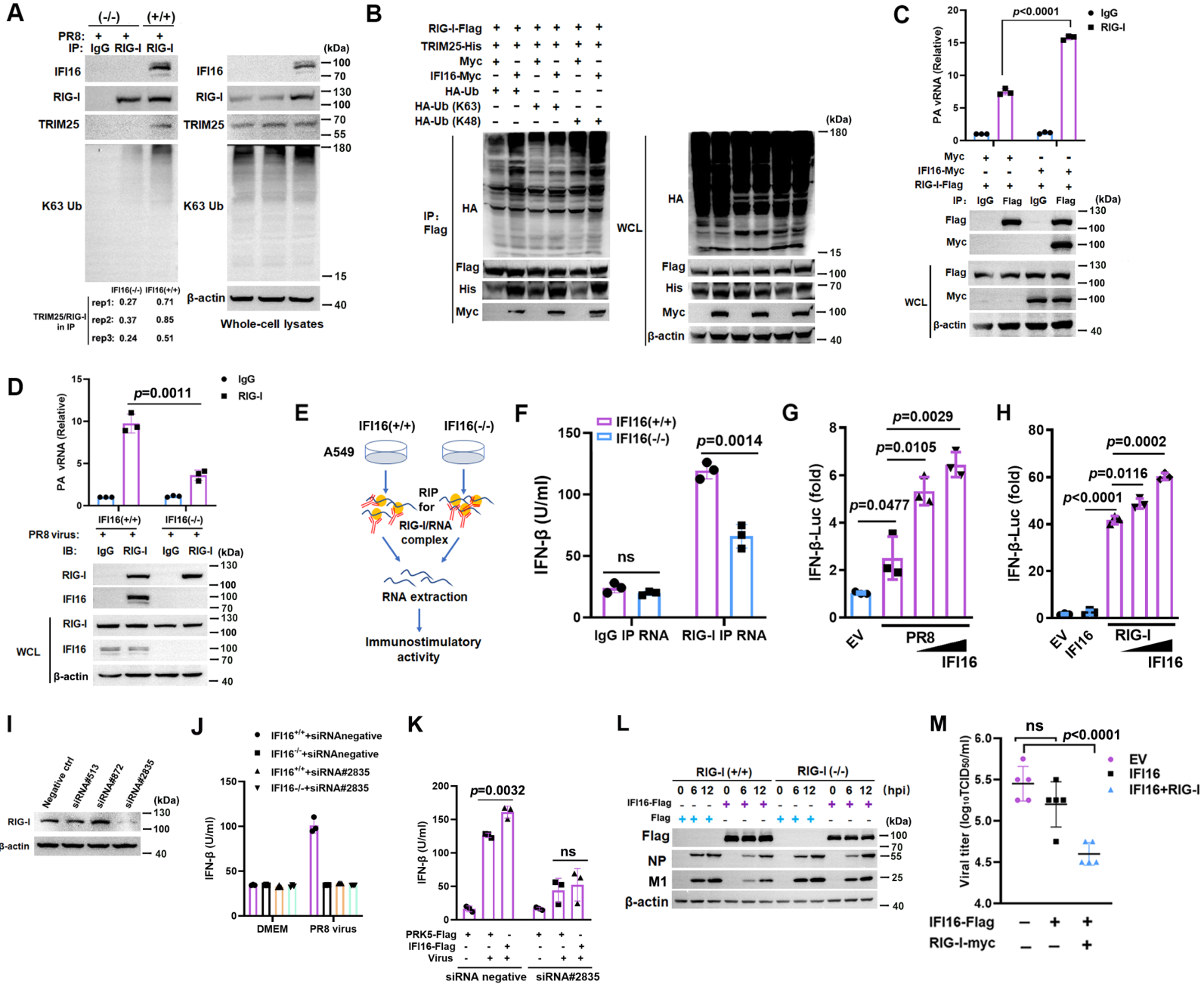












Influenza A virus



IFN- α/β

IAV genome RNA

